Ionization of Stretched Hydrogen Atoms by Collinear Microwave and Static Electric Fields

J. E. Bayfield, S. Y. Luie and L. C. Perotti

Department of Physics and Astronomy, University of Pittsburgh

Pittsburgh, Pennsylvania 15260

ABSTRACT.

Microwave ionization of stretched highly excited hydrogen atoms is studied experimentally, for the case of a linearly polarized microwave electric field superimposed with an uniform static electric field. Both fields are collinear with the direction of atom stretch. As evidence exists that the system can be semiclassical for ionizing field strengths, model numerical calculations based on the classical physics are reported. As the microwave field is pulsed with a half sinewave pulse envelope, classical processes induced by the pulsing are explored. These are found to be very important. The nature of these processes is revealed by the technique of overlaying snapshots of the phase space location of the classical ensemble of electron trajectories on top of corresponding surfaces of section. For fixed values of scaled peak microwave field strength F_0, experimental and numerical values of the ionization probability P_I were obtained as a function of scaled

microwave frequency ω_0' over the range 0.56-1.17, in steps smaller than 1%. For F_0 = 0.02 and the frequency range ω_0' = 0.8-0.9, the ionization is nearly classical; it is initiated by the classical process of electron probability flow into a chaotic band in phase space. At the lower edge of this frequency range, numerical values of the ionization probability show extreme sensitivity to small amounts of microwave noise. This occurs because a change in evolution occurs near an unstable fixed point. The flow into the chaotic band is initiated by a transition of the electron trajectory ensemble from a location near a stable manifold to motion parallel to an unstable manifold. Outside the frequency range, values of P_I are small, but larger than classical values. When F_0 = 0.03, the nearly classical region enlargens to ω_0' = 0.72-1.08. The classical process of separatrix-crossing during the rise of the pulse produces resonance island trapping at the higher frequencies within this frequency range. Above ω_0' = 1.08, P_I now has values smaller than classical. At still higher fields, $P_I(\omega_0')$ becomes large within the entire frequency range under study and exhibits both more nearly classical structure and more nonclassical structure. The threshold field strength for ionization also was measured as a function of frequency. Results are compared with previous data obtained with a beam of atoms having only the principal quantum number well-defined. Present results with stretched atoms display considerable structure that was either absent or weakly present in the previous work. Within a certain frequency range below the region of trapping within the primary resonance island, threshold fields for ionization are in close accord with an expression for the location of the separatrix zone.

1. Introduction

Few things would seem more fundamental in the physical world than the time evolution of quantum mechanical systems. Yet much is not known about the impact of nonintegrable Hamiltonians on the evolution prescribed by Schroedinger's equation. Since the discovery of nonperturbative microwave ionization of highly excited hydrogen atoms and its resonant frequency dependence [1], many theoretical investigators have demonstrated relationships of this ionization to the dynamics of the corresponding nonintegrable classical system. Comparisons of quantum and classical numerical calculations have played a pivotal role [2,3]. Since quantum calculations in more than one spatial dimension have been difficult, such comparisons usually have employed one dimensional models to obtain quantum ("Q1D") and classical ("C1D") results. Three dimensional classical ("C3D") Monte Carlo calculations also have been possible.

The C1D results reveal characteristic zones in both the electron location (x,p,t) and action-angle (θ,I,t) generalized phase spaces. Zones of regular electron motion include those occupied by nested vortex tubes and those of the field-modulated atom [4]. Chaotic zones include both zones of local chaos and of global chaos. Parameter values exist where zones of "local" and global chaos touch, but yet the "local" chaos zone can be distinguished by much longer average characteristic electron escape times [5]. Stroboscopic surfaces of section reflect all these zones in the full (θ,I,t) phase space as characteristic zones in the action-angle (θ,I) subspace, the vortex tubes producing resonance island zones and the local chaos producing zones of irregular motion that have been loosely termed "separatrix" zones [6]. (Classically the separatrix in integrable

problems becomes "broken" in the nonintegrable driven hydrogen atom problem to become a chaotic layer that grows in size with increasing microwave field strength.) Important Q1D results show that the classical zones in phase space are reflected in the character of the semiclassical Floquet eigenstates (SFEs) [4]. Thus regular SFEs can be either resonance island SFEs or modulated atom SFEs. Irregular SFEs include the separatrix SFE, possibly "scarred" by a high electron probability density in phase space along an unstable periodic orbit [7]. At intermediate values of microwave field strength, scarred separatrix SFEs exhibit partial quantum localization about the unstable periodic orbits (rather than marked localization about nested vortex tubes), and otherwise are distributed mostly throughout a bounded region of phase space classically occupied by chaotic trajectories (a region of local chaos) [4]. At higher field values, the local and global regions become less distinguishable, and some portion of a separatrix SFE may become noticeably delocalized.

Considerable progress also has come from comparisons of numerical results with data from experiments utilizing fast atomic beams passing through microwave cavities or waveguides. In such experiments, hydrogen atoms are excited, exposed to the microwaves, and then checked for ionization. The time sequence arises from atom passage through different spatial regions in turn. Three dimensional ("E3D") experiments utilize ensembles of atoms initially having a defined principal quantum number n and an approximately statistical distribution over the other quantum numbers [8]. Comparisons of Q1D results with E3D data have been qualitatively successful in explaining the parameter dependence of low ionization probabilities [3]. One suggested reason for this is that the

most easily ionized states within a given Stark energy level manifold with a single value of n are the lowest lying (stretched atom) ones. In addition, it has been suggested that for sufficiently short microwave pulses the applied linearly polarized microwave electric field is so strong and the microwave energy absorption process so rapid that only the component of the electron motion along the field direction is significantly modified.

A second experimental approach adds a uniform static electric field to the system. This field is present over the entire evolution of each excited atom, beginning with its laser excitation to a single stretched atom energy eigenstate and ending with its contribution to the measurement of the microwave-induced distribution of final stretched atom states in the atomic beam [9-11]. In such nearly one dimensional ("E1D") experiments, the rapid quantum flow of probability primarily over the single ladder of extremal Stark (stretched atom) states can be close to that of 1D quantum models [12,13]. The experimental evidence for this is sharp steps with increasing analyzer field strength in the survival probability for the atoms passing through a state-analyzing static field region following the microwave interaction region [11]. Each step is the removal of those atoms having one value for the prinicpal quantum number.

One remarkable finding of the E3D experiments was the presence of local maxima in the microwave frequency dependence of the microwave field strength F(10%) for 10% ionization probability [14]. These maxima are called regions of local stability in the microwave ionization threshold field values. Some of them were found to be reproduced well by C3D calculations, and therefore are called regions of classical local stability ("regions of CLS"). C1D results indicate that such regions are associated with resonance

island zones. However, a different E3D region of local stability was not reproduced by classical calculations, but was found in Q1D results [3]. Further Q1D calculations for this region of quantum local stability ("region of QLS") found a high probability amplitude for one scarred separatrix SFE at the peak of the E3D experimental microwave pulse. This interesting linkage of a special Q1D SFE with a specific E3D region of QLS has yet to be explained in terms of the three dimensional quantum evolution.

The reasons for the preferential creation of specific SFEs near the peak of the microwave pulse are now being explored. During the rise of the microwave pulse, an initially regular classical initial state (the set of initial conditions for an appropriate ensemble of electron trajectories) can evolve into a separatrix zone and subsequently flow within it [15]. Quantum mechanically this process involves the population of separatrix SFE's when the instantaneous field reaches values for the classical transition into the separatrix zone [16]. In addition, such a zone classically may be completely traversed to reach a classical state evolving on nested vortex tubes. This process is called "separatrix crossing" [17], and it can produce temporary partial ensemble trapping within nonionizing classical states. This is a classical mechanism for the quantum system to evolve into resonance island SFE's near the peak of the pulse, producing "island trapping" that suppresses the ionization. Separatrix crossing during both the rise and fall of the pulse is one mechanism for the near-classical characteristic structure in final bound state distributions that has been observed in E1D experiments [15].

Very recently it has been demonstrated by both Q1D and Q3D calculations that both resonance island SFEs and separatrix SFEs may evolve as nondispersive wave packets

[18,19]. This is believed to be due to a compensation of the free atom energy level anharmonicity by the atom interaction with the microwave field. This finding provides new motivation for further experimental and theoretical investigations of the efficient population of such Floquet eigenstates.

In Section 2 of this paper, we describe the apparatus we have used in our E1D experiments, along with some tests employed to assure its proper functioning. In Section 3 we outline our procedures for the classical calculation of ionization probabilities, employing a 1D model that includes the effects of the static electric field. We describe the numerical procedure we have developed for identifying classical transport processes induced by the rise of the pulse. As a function of time into the pulse, snapshots of the trajectory ensemble are compared with corresponding fixed-field stroboscopic surfaces of section. Examples are given for ionization triggered near an unstable fixed point, producing flow following an unstable manifold. Also demonstrated is ionization suppression (CLS) due to separatrix crossing that results in island trapping. These transport processes, and combinations of them, are used in the following sections to help explain some of the experimental observations.

Section 4 presents our experimental results for F(10%) and compares them with previous E3D data taken at zero static field strength. Previous hints of some structures in F(10%) are strongly confirmed. Of particular interest is a high field region of local stability, associated with the lower branch of a separatrix zone, located below the primary nonlinear resonance zone.

Section 5 presents extensive data for ionization probabilities higher than 10%. Comparisons of such data are made with one dimensional numerical predictions, a procedure at present justified only for the case of E1D experiments. Fluctuations often larger than corresponding C1D classical ones are observed in the field strengths required for 30% and 60% ionization probability. These are quite sensitive to the parameters. Ionization probabilities for fixed values of scaled field strength are also presented. These include low field values where there is experimental ionization but no classical ionization within large frequency ranges. The fixed-field results sometimes exhibit more clearly the regions of stability than do results for field strengths at fixed ionization probability, for regions of stability may be missed in the latter if the field strength does not happen to be appropriate. A number of ionization extrema in the frequency dependence $P_I(\omega_0')$ are consistent with classical explanations. A comparison with C1D and Q1D calculations indicates that one strong ionization minimum is due to quantum suppression (QLS). Very close to the center of the primary resonance zone, strong non-classical variations in the ionization are observed as the initial value of the atomic principal quantum number is changed. This is consistent with recent theoretical predictions of special quantum behavior of some SFEs in this frequency region. The impact of our results for future studies is discussed briefly in Section 6.

2. Experimental Techniques

Present limitations on the CW laser technology available for exciting atoms make difficult the production of adequate numbers of state selected, highly excited, thermal

velocity hydrogen atoms. Because of this, a refinement of the fast atomic beam techniques utilized in the original microwave ionization experiments [1] has occurred. Still utilized is the highly excited state content inherently present in the hydrogen atom beam produced by charge exchange collisions of a ~20 keV proton beam passing through a low pressure gas. A first enhancement of both highly excited state density and state selectivity was achieved by introducing a grating tuned, single longitudinal mode CW CO_2 laser [20]. This laser excited a portion of those 0.04% of the atoms having principal quantum number n = 10 into states with a selected much higher value n_0. For a proper choice of atomic beam kinetic energy, sending the laser beam collinear with the atom beam enabled Doppler tuning of the atomic frequency into resonance with the laser frequency. Further enhancements came from the introduction of a optical double resonance (ODR) laser excitation technique [21]. This utilized two sequential CW CO_2 laser transitions in separate static electric fields, beginning with n = 7 atoms in the beam. Figure 1 schematically shows how we employed this technique in the present experiments. Except for the sign of the atomic azimuthal quantum number m, the n=7 to n=10 transitions are completely resolved at a sufficiently high static fields. For m=0, this completely state selective technique has been a mainstay of both the nearly 1D and 3D microwave ionization experiments carried out to date. Details of the ODR technique are well described in the literature [22].

In 3D experiments, the ODR selection of parabolic quantum numbers to be n_1=0, m=0 is deliberately undone by passing the atoms into a spatial region of nearly zero static field. Residual stray fields then produce an ensemble of atoms believed to be statistically spread

over all values of n_1 and m. In contrast, the present nearly 1D experiments maintained a constant nonzero static field large enough to overcome stray fields. This maintained the selected values of quantum numbers [9,11]. The schematic of our present apparatus, shown in Figure 2, indicates how this is done. The proton beam is created in the region "1" and converted by charge exchange and proton deflection into a pure atomic beam at "3". At this point a 110 kV/cm static field between wire electrodes was used to field ionize at least 99% of the unwanted n=10 atoms coming from the charge exchange gas cell. The history of each atom then evolved because of its motion further to the left in Figure 2. The atom beam is almost collinear with a 30 watt laser beam originating from the laser labeled "15".

The high directed velocity v of the fast atoms was combined with a transverse uniform magnetic field B in the laboratory to produce a constant transverse motional electric field $F_S=vxB$ in the atoms' rest frames. The large rectangular coils labeled "14" produced the magnetic field. It was uniform beginning within the strong field parallel plate aluminum electrodes labeled "4" where the n=7 to n=10 transition takes place. This uniform field continued to the left, up to the region labeled "10", where all the highly excited atoms are field ionized for detection purposes. The laser excited atoms passed near no magnetic materials during their history. Thus F_S is an adjustable constant component of the instantaneous vector static electric field throughout that history. This includes the time evolution of the atoms during passage through the OFHC copper WR-62 rectangular microwave waveguide "7", where in their rest frames they are exposed to a half sinewave pulse of microwave electric field linearly polarized parallel to F_S. The magnitude of the

magnetic field B was measured to within ± 2%, using a Hall effect gaussmeter calibrated against a reference magnet. These measurements were carried out after the two components of the earth's magnetic field transverse to the atom beam axis were canceled out to within ± 10 mGauss, using other very large rectangular coils far outside the apparatus.

The highly excited atoms were detected by passage through the final portions of the apparatus, beginning with the axial field structures labeled "9". Their conversion into protons occurred within and just in front of a OFHC copper cylindrical microwave cavity aligned collinear with the atom beam and operated in the TE_{111} mode at 8.34 GHz. Employing a standard technique, a low "proton energy label" potential was applied to the cavity relative to its vacuum chamber. Those neutral atoms that entered the ionizing cavity and left it as protons acquired a kinetic energy boost equal to the change in electrostatic potential energy. Region "9" contained a series of parallel apertures connected to a resistance divider chain, bringing the cavity vacuum chamber potential above machine ground. For fixed cavity label potential, this reduced the static electric field in front of the cavity, thereby reducing atom field ionization outside of the cavity. The highest principal quantum number of atoms detected using this apparatus was determined by the larger of the static fields in region "9" and in front of the cavity within its chamber, both added vectorially with F_S. For most of the data to be presented in this paper, this quantum number was $n_c = 90 \pm 3$. The lowest quantum number of the detected atoms was determined by the strength of the cavity microwave electric field. This number was determined by preparing atomic beams with different values of principal quantum number,

and varying the cavity field to observe saturation of the field ionization signal. At least 90% of atoms with $n_b \geq 50 \pm 3$ were detected. **Thus "ionization" in the case of most of our results means transition out of the band of principal quantum numbers between 50 and 90.**

Protons leaving the cavity ionizer region "10" were charge separated from the atomic beam using a large parallel plate electrostatic analyzer [23,24]. The transmitted protons then passed into a "filter lens" axial field parallel aperture structure [25]. It had a maximum positive electrostatic potential on its central aperture and resistance divider strings on each side string of apertures. The central aperture potential was set for maximal transmission of the cavity labeled protons that were produced when the cavity microwave field was turned on. Unlabeled protons were turned back by the central aperture potential, reducing by orders of magnitude their background contribution to the proton current measured by the Johnston MM-1 electron multiplier labeled "12" in Figure 2.

Analog phase sensitive detection was employed to increase further the signal to background. A mechanical chopper was inserted in the laser beam just before it entered the vacuum system at the right side of Figure 2. Its electronic output signal was used as the reference signal to an electronic lockin detector, whose input was the electron multiplier anode current. A chopping frequency near 190 Hz optimized the lockin signal to background to a value typically near 30.

The collimations of both the atom beam and laser beam were critical aspects of the experiments. Collimation of the atom beam was varied by changing a first collimator in the vacuum chamber between the ion source "1" and the ion-beam bending magnet "2" used

to separate protons from other ions in the beam coming from the ion source (see Figure 2), and by changing the second collimator which was an 5 mm diameter insert in the exit end of the charge exchange gas cell in the center of region "3". By changing the diameters of these collimators by a factor of three and studying the resultant changes in transmitted ion beam profiles obtained by scaning the bending magnet, it was ascertained that the collimation of the proton beam was not seriously affected by the dispersion and defocusing introduced by the bending magnet. However, an increase was detected in the angular divergence of the atom beam over that of the proton beam, as detected using the partial stripping of atoms in the background gas in the apparatus. This increase was caused primarily by the charge exchange collision process. It introduced limitations on the applicability of our present techniques. A 5.0 mm diameter waveguide post-collimation aperture was carefully centered on the atomic beam axis, in front of the 5.8 mm diameter beam entrance hole electric discharge machined in the narrow side of the waveguide. A small portion of the atom beam striking the post-collimation aperture produced a secondary electron emission current that was monitored. The post-collimation aperture was mechanically cleaned at the beginning of each series of runs. During a run the state purity of the highly excited atom beam was monitored by comparing field ionization curves obtained using plate pairs before and after the waveguide, see below. As a run progressed, state purity at high values of n_0 was observed to deteriorate, a process that could be reversed by a new cleaning of the post-collimation aperture. Our studies using our much smaller proton beam collimator apertures reduced the post-collimation aperture secondary electron current by at least four orders of magnitude. However, this did not

eliminate the time-dependent deterioration of state purity, which apparently was produced by stray electric fields arising from post-collimation aperture chargeup. This effect limited the highest values of n_0 that could be studied to about 76. Extension of nearly 1D experiments to higher values of n_0 will require final and complete collimation of the atom beam before the excitation from n=10 to $n=n_0$, a change that will require major reconstruction of the apparatus.

The 3 mm diameter laser beam diverged from the laser with a half angle of about 3 mrad. It was recollimated by the atom beam collimator at the exit end of the gas cell. The observation of a spot on the post-collimation aperture produced by the laser beam indicated that its nominal diameter at that aperture was 5 mm. Tests verifying that this estimate is adequate are described below.

Figure 2 also shows some of the parallel plate electrode structures placed along the beam line between "4" and the beginning of the field ionization region "10". These structures all were carefully constructed and aligned, so that the field nonuniformity within them was due to the finiteness of the plate areas. Table I lists the lengths of the plate pairs and our names for them, going from right to left in Figure 2. Further details of the plate pairs, the regions between them and their alignment are available [26]. When the highly excited atom signal was being measured, the potentials on all the plates were zero except for the high field plates "4".

The preionizer plates were just before the microwave waveguide, the post-ionizer plates just after. Note that the listed plate lengths are large in comparison with the 15 mm width of the microwave waveguide. The last three sets of listed plate pairs each were used

as field ionizers to explore the highly excited atom beam intensity and state content at their beam entrance locations. With the microwave field turned off, normally all these plate pairs produced the same dependence of field ionization probability on field strength. Comparisons of the data obtained with the different plate pairs demonstrated that with a clean waveguide post-collimator aperture, initial state purity in n_0 (and at least 80% substate purity, see below) was achieved for n_0 between 57 and 76.

Sometimes effects of laser excitation within plate pairs were observed when using the preionizer plates. However this never occurred using the post-ionizer or state analyzer plates. This observed absence of such effects along with the equality of highly excited atom beam intensity observed with the post-ionizer and state analyzer plate pairs showed that very little of the laser beam was passing through the microwave waveguide. This was the result of a deliberate rotation of the laser beam axis relative to the atomic beam axis by about 3 mrad, so that the laser beam was just intercepted by the waveguide post-collimator aperture. This was done to reduce the probability of possible laser excitation within the waveguide when the microwaves were on, below the nominal 5% value determined by the ratio of the waveguide width to the sum of the low-field shield plate and preionizer plate lengths. (Since the extemal Stark state $n=10$ to $n=n_0$ transition moment responsible for the excitation before the waveguide is the largest moment of all substate transitions between the two manifolds of Stark energy levels [27], it is very unlikely that laser excitation within the waveguide would have a much larger moment.) Routine checks showed that application of a preionizer field just adequate to fully ionize the atomic state

produced by the laser excitation did reduce the highly excited atom signal below the 3% level of the signal detection system noise.

Our ability to completely resolve components of the atomic beam having different n has been demonstrated previously [9,11]. In Figure 3 we present further evidence of the degree of substate selection achieved using our techniques. The solid line is an experimental analyzer plate scan of the signal produced when n_0=72 atoms are prepared. For a single substate atomic beam and analyzer plates of infinite transverse extent, this 50% point on this scan can be computed to be 23.5 V/cm using a semiempirical formula of demonstrated applicability [28]. The 50% point of the data in Figure 3 lies at 23.7±0.4 V/cm. The uncertainty indicated arises from the uncertainty in the analyzer plate spacing. However, the shape of the scan is not perfectly reproduced by the formula, either because of substate impurity, transverse field nonuniformity or both. Both effects would raise the voltage needed on the plates to produce a given amount of field ionization. Assuming no field nonuniformity, we have fitted the experimental scan to various substate impurity distributions and levels. The dots in the figure were obtained for a distribution of 80% $(n,n_1,m) = (72,0,0)$ states and the remaining atoms distributed uniformly in n_1 up to n_1=10 with m remaining zero. This 80% is only a lower bound on state purity, as the field nonuniformity is estimated to be important. Its inclusion would raise the bound.

Figure 4 shows the microwave system used for producing the microwave field within the waveguide. The 12.4-18.0 GHz source of microwaves was a Hewlett Packard 8672A frequency synthesizer amplified by a Hughes 20 watt traveling wave tube amplifier, the latter also being an 8 mW source of broadband microwave noise. The amount of noise

incident on the atoms was limited by a broad band reflective filter to be within the 12.4-18.0 GHz frequency band. Trading off the settings of the coaxial attenuators shown in Figure 4 permitted adjustment of the ratio of noise field to sinewave field over the range of 0.05% to 10%, the minimum noise power being 6 μW. Adding the tunable narrow bandpass filter presumeably reduced the noise power to 0.6 nW while reducing the 3 dB bandwidth of the microwave system to 30 MHz. Its rejection was 40 dB at ±150 MHz from the center frequency. It was observed that setting the second coaxial attenuator to high attenuations then reduced the noise power level to less than 10 nW. Without the narrow bandpass filter, a Tektronix 2750 spectrum analyzer was used to monitor the microwave frequency spectrum.

A calibration of the microwave electric field strength seen by the atoms passing through the microwave waveguide was carried out before and after the experimental runs. The procedures that were utilized have been documented in detail [29]. In brief, the various transmissions of the directional couplers and microwave windows shown in Figure 4 were separately measured over the 12.4-18.0 GHz frequency band using three different Hewlett Packard 8478B thermistor power meters to check for power meter variations. Then this calibrated equipment was utilized to measure the frequency dependence of the transmission of the interaction waveguide itself. The average of the incident and transmitted microwave powers for the waveguide was taken as determining the microwave field seen by the atoms. The frequency dependence of this average was used to correct the power meter averaged experimental field value obtained at 15.0 GHz. The values of microwave fields so obtained were estimated to be accurate to within ±12%.

The ~6% changes in the calibrations obtained before and after the runs are included in this uncertainty.

For the present microwave ionization studies, our data acquisition system was simple. The parameters for a series of runs would be selected and the tests mentioned above performed. A set of five minute scans of the waveguide microwave power would be carried out by varying the first variable attenuator shown in Figure 4. The microwave power and the highly excited atom signal from the lockin output were simultaneously recorded on a XY recorder. Figure 5 shows a few of these "ionization scans". For a given set of parameters, several scans would be overlayed and then averaged by eye, and the mean power for 10% "ionization" probability ascertained. This could be converted to the threshold field F(10%) for "ionizaton" using the known relationship between incident waveguide microwave power and the microwave field strength in the atom-field interaction region.

3. The Numerical Calculation of Classical Microwave Ionization Probabilities.

One motivation for carrying out nearly 1D experiments is to further understanding of the relationships of the quantum and classical dynamics of nonintegrable semiclassical systems. The simplest physical systems that display all the generic types of classical dynamics have a 3D phase space, e.g. are conservative systems in two spatial dimensions or are explicitly time dependent systems in one spatial dimension, such as the present one. Only in such systems can one explore the full 3D phase space by computing 2D surfaces of section. Adding just one more spatial dimension would result in a 5D phase space, which

makes a complete analysis of the dynamics of the system intractible, classically as well as quantum mechanically. Thus the degree of one dimensionality of our system is of considerable interest, and comparisons of E1D data with Q1D and C1D results are valuable.

The stretched highly excited hydrogen atom has an electron probability distribution strongly displaced to one side of the atomic nucleus, producing a large electric dipole moment extremal within a Stark manifold of states [30,31]. At our values of n_0, the classical electronic Kepler orbit is highly elongated, with an outer turning point at about 400 nm from the nucleus and passage around it at distances of about 0.3 nm [32]. The Coulomb field at 0.3 nm is about $2 \times 10^{+8}$ V/cm, 10^{+7} times the microwave field values of interest. Thus it is reasonable to ignore the microwave field at these short distances, and furthermore ignore the short purely Coulomb "wrap around" portion of the electron trajectory about the nucleus. This is the justification for employing the surface state electron (SSE) 1D model for the classical motion, where the electron is allowed to move only on one side of the nucleus [33]. Including a term for the energy of a stretched atom in the static electric field F_S, the SSE Hamiltonian in atomic units becomes

$$H = p^2/2 - 1/z + z[A(t)F\sin(\omega t + \phi) - F_S],\ z \geq 0, \qquad (1)$$

where A(t) is the envelope of the microwave pulse and the dipole gauge chosen is a good approximation when $(1/A)(dA/dt) << \omega$ [34].

We transform to free-atom action angle variables (I,θ), valid when the electron's energy is negative, by first introducing the eccentric anomaly angle $\xi(\theta)$

$$\theta \equiv \xi - \sin\xi$$

$$z = 2I^2 \sin^2(\xi/2)$$

$$p = (1/I)\cot(\xi/2)$$

To avoid equations of motion that contain terms that diverge as z approaches zero, a dummy time η is introduced according to [35]

$$dt \equiv (1 - \cos\xi)(d\eta).$$

The true time t increases monotonically with η. Newton's equations of motion then become

$$\begin{aligned} dI/d\eta &= -I^2 \sin\xi[A(t)F \sin(\omega t + \phi) - F_S] \\ d\xi/d\eta &= 1/I^3 + 2I(1-\cos\xi)[A(t)F \sin(\omega t + \phi) - F_S] \\ dt/d\eta &= 1 - \cos\xi \end{aligned} \qquad (2)$$

To closely simulate the experimental situation,

$$A(t) = \sin(\pi t/T_p)$$

where T_p is the length of the microwave pulse. The above three ordinary differential equations were numerically integrated for an ensemble of initial conditions (θ_0, I_0) that was constrained by the requirement that to first order in F_S the (classical) electron energy E is equal to the value of the energy of the experimentally prepared initial quantum energy eigenstate

$$-1/2n_0^2 - (3/2)F_S n_0^2 = E = -1/2I_0^2 - F_S I_0^2(1 - \cos\xi_0) \qquad (3)$$

Given a value of $\theta_0(\xi_0)$, this equation determined a corresponding value of I_0.

The equations of motion (2) were numerically integrated using a fixed step, fourth order Runge-Kutta routine. Two different codes were independently written, one utilizing

subroutines from the Numerical Recipies collection [36], and the other not utilizing any such previously published code. The two codes produced the same results to within four decimal places. Our calculations reproduced results of previous investigators [3].

Several types of calculations were carried out. Fixed-ϕ stroboscopic surfaces of section of the long-time evolution in (θ,I) space were computed for A(t) equal to various constants. These revealed the long-time structures existing in phase space for the various values of F instantaneously traversed during the microwave pulse. Fixed-ϕ instantaneous distributions in (θ,I) were obtained including the pulsed A(t), for instantaneous values of A(t) equal to those for the long-time surfaces of sections. This enabled us to compare instantaneous distributions with long time surfaces of section, for various times t during the pulse.

Classical values for the "ionization" probability P_I at the end of the pulse were computed, taking averages over at least 300 initial conditions spanning at least 15 equally spaced values of ϕ and least 20 equally spaced values of θ_0. The "ionization" probability contained two contributions. One came from trajectories that were terminated at some time during the pulse where the instantaneous value of the energy E exceeded the value $1/9I^4$ for rapid ionization in the static field alone. The other contribution was from trajectories whose final value of E corresponded to energies of quantum energy eigenstates, see equation (3) above, with quantum numbers outside the interval [50,90] defining the experimental "ionization". Calculations of P_I for numerous values of F enabled us to determine C1D numerical values of F(10%), the pulse peak threshold microwave field for "ionization".

In this paper we present our findings in terms of classically scaled parameters. Noting the classical-quantum correspondence n=I in atomic units, the Hamiltonian (1) can be written as a scaled Hamiltonian H' by introducing the scaled variables $p'=n_0p$, $z'=z/n_0^2$, $t'=tn_0^3$:

$$H' \equiv n_0^2H = (p')^2/2 - 1/z' + z'[\sin(\pi t'/T_p')\, F_0\sin(\omega_0 t' + \phi) - F_{S0}],$$

where the scaled microwave field strength is $F_0 = n_0^4F$, the scaled static field is $F_{S0} = n_0^4F_S$, and the scaled microwave freqency $\omega_0 = n_0^3\omega$. For values of $\omega_0 < 0.7$, 3D experiments have found that the major effect of introducing F_S on the unscaled ionization threshold fields F(10%) is the first order Stark shift of the atomic resonance frequencies [8]. Thus we present our data in terms of the Stark corrected scaled frequency [3]

$$\omega_0' = \omega_0/(1 - 3F_{S0}).$$

As an example of our classical numerical results for ionization probabilities, Figure 6 shows panoramas at different fixed values of F_0, for the values of F_{S0} and T_p' utilized in our $n_0 = 69$ experiments. At $F_0 = 0.015$ the probability is nonzero only between scaled frequencies ω_0' of 0.8 - 0.9, while at $F_0 = 0.063$ the probability is close to one except for frequency regions near 1/2 and 1. At various intermediate fields there are also marked ionization minima (classical local stability) near ω_0' = 2/5, 2/3, 4/3 and 3/2, as well as ionization maxima near ω_0' = 0.44, 0.57, 0.61 and 0.69.

Using the technique of comparing classical trajectory ensemble snapshots with corresponding stroboscopic surfaces of section as described above, we have demonstrated that all these minima are due to partial ensemble trapping within island (chains), and that all these maxima are due to ensemble destabilization near unstable fixed points [17]. As an

example of destabilization dynamics, Figure 7 shows the case for p/q = 1/2. Figure 8 shows trapping, again for p/q = 1/2. Figures 9a,b show trapping at one moment of time for p/q = 4/3. Similarly, figures 9c,d show a partially destabilized ensemble due to the p/q = 2/3 unstable fixed points, along with the corresponding surface of section. In this last case, portions of the ensemble lie near both the stable and unstable mainfolds, nicely outlining the p/q = 2/3 resonance zone that contains both regular and locally chaotic parts. Table II enumerates the field and frequency values where trapping or destabilization have been observed in these classical calculations. It is interesting to note that parameters have been found where trapping and destabilization of different portions of a single ensemble both occur, either sequentially or almost simultaneously.

4. The Frequency Dependence of the Threshold Microwave Field Strength for Ionization.

Experimental ionization curves over the frequency range ω = 12-18 GHz have been obtained for n_0 = 60, 65, 69 and 72. The static field F_S was fixed at 8.0 V/cm. As the Doppler effect had to be utilized to fine tune the second laser excitation process into resonance, slightly different atom beam energies were used for the runs with different n_0, 22.3, 21.7, 21.4 and 19.15 keV respectively. The corresponding unscaled microwave pulse times T_p are 7.64, 7.75, 7.80 and 8.23 ns, and the scaled times T_p' then are 146.2, 116.7, 98.2 and 91.2 respectively. Furthermore, as ω was varied over its 50% range, the pulse time in units of the microwave period varied significantly, for instance from 90 periods to 135 periods. Nevertheless, our results for the ionization threshold fields shown in Figure 10 exhibit a remarkable degree of classical scaling, for 4% to 8% changes in n_0.

This indicates that these classically scaled threshold data are fairly insensitive to simultaneous increases in F_{s0} and T_p' of typically 24% and 18% respectively.

Figure 10 also shows a comparison of our threshold data with the structure in previous E3D data obtained using microwave cavities at fixed ω, F_s very close to zero, a fixed pulse envelope with a flat top, various values of n_c and n_0 stepped over various relatively large ranges. The values of ω are 9.923 GHz [37], 36.02 GHz [38] and 9.904 GHz [39]. To obtain the comparisons in structure shown in Figure 10, we have used a "mixed-units" plotting procedure for the E3D data (only), which has been shown to account for the effects of the static field on E3D ionization threshold data for frequencies below 0.7 [8]. Thus for the E3D data, the vertical axis of the figure is proportional to unscaled microwave field, here in units of the scaled field for $n_0 = 69$. To produce the curve shown for 36.02 GHz, division by the additional resonance quantum number factor $[n_{r,9.91} / n_{r,36.02}]^4 = (36.02/9.91)^{4/3} = 5.59$ was included. All of the results shown in the figure exhibit stability (a maximum) near $\omega_0' = 1/1$, except for the 9.923 GHz data. It is believed that the latter data suffers from $n_0 = 87$-90 being too close to the cutoff $n_c = 94$ [8]. A comparison of the 36.02 GHz data to the results of C3D Monte Carlo calculations has shown very close agreement, leading to the explanation that this peak is due to a nearly classical mechanism that produces classical local stability [38].

All the results shown in Figure 10 also show a minimum near $\omega_0' = 0.84$ and a large rise in F(10%) as ω_0' is further reduced to 0.55. The minimum defines the center of a region of "easy ionization". The classical ensemble destabilization mechanism for this ionization was discussed near the end of section 3, see also Figure 7. The present E1D

data also show two local maxima near $\omega_0' = 0.63$ and 0.69. We note that for each of these relatively wide maxima, two out of three of the E3D curves exhibit hints of them. Also there are signs of fine structure within the E1D $\omega_0' = 0.69$ peak. As noted in Section 1, previous investigators have found some evidence that a maximum at $\omega_0' = 0.56$ is due to a nonclassical mechanism that produces a "region of QLS" [41]. We shall show in Section 5 below that the peak near 0.69 also is very likely such a region.

Although we could carry out E1D experiments only for $n_0 \leq 76$, we have made non-1D measurements at $n_0 = 80$ with F_S reduced from 8 V/cm to 1 V/cm. The reduction enabled an increase in n_c from 90 to 110. The results for the frequency range between $\omega_0' = 1.31$ and 1.42 are interesting, as seen in Figure 11. There is a peak within this range, containing a sharp central maximum located at $\omega_0' = 1.37$. Our C1D calculations do not show any of these features, so again we have a region of QLS. A similar feature (without the sharp central maximum) centered at $\omega_0' = 1.33$ in the E3D data is the one mentioned in Section 1, as being associated with the population with 96% probability of a scarred separatrix SFE at the peak of the microwave pulse. Thus a candidate explanation of our data in Figure 11 is the transient creation of such a state with high probability amplitude.

The identification of the $\omega_0' = 1.33$ peak in the E3D data with the separatrix zone is supported by an approximate calculation of the area of the primary resonance zone that is based upon a modified pendulum approximation [40]. An integrable local approximation of the Hamiltonian (1) (with A(t) a constant and $F_{s0} = 0$) is made around the resonant action I_r defined by the condition $1 = \omega I_r^3$ [35]. In brief, the free atom hamiltonian is expanded in powers of $(I - I_r)$ through second order and the atom-field interaction term is

Fourier expanded in the angle variable θ. All terms of the latter expansion except the first one average to zero over one period of the microwave field. Thus they can be neglected in a first approximation. The fast motion with frequency ω can be removed by a canonical transformation that eliminates the time dependence of the interaction term. This also eliminates the linear term in the expansion of the free atom Hamiltonian, leaving the Hamiltonian of a pendulum that describes the slow motion inside the resonance island. The small extra cubic term in $(I - I_r)$ then is included to take into account the asymmetry in action of the resonance zone.

A similar treatment that includes a static electric field while omitting the asymmetry term is discussed in [16]. The result can be easily extended to include that term, yielding the following formula for the "separatrix actions" $I^{\pm}$ defining the top and bottom boundaries in action of the $\omega_0' = 1$ resonance zone:

$$I^{\pm}/I_r = 1 \pm (4/\pi)B^{1/2}(F_r)^{1/2} + (4/3)BF_r/(1+F_s^r)\,, \qquad (4)$$

where $B = 0.325/[3(1+F_s^r)(1-3F_s^r)]$. Here F_r and F_s^r are the microwave and static fields scaled by I_r^4, now given by the condition $1 = \omega I_r^3/(1-3F_s^r)$. Equation (4) can be used to estimate the location of the separatrix in the ω_0', F_0 parameter space. One introduces $x=I/I_r$ as a parameter, and numerically inverts equation (6) (with the + sign if $x > 1$ and viceversa) to obtain $F_0 = x^4 F_r$. Now ω'_0 will be given by $\omega'_0 = x^3(1-3F_{s0}/x^4)/(1-3F_{s0})$. The locus of points ω_0', F_0 so obtained we call the separatrix location function. A

comparison of a plot of the separatrix location function for the lower separatrix with the experimental data for $F_0(10\%)$ versus ω_0' is made in Figure 12. Since the data was taken for two different values of the principal quantum number, the two corresponding location functions are shown. The agreement is quite good. The rise in Figure 12 of the experimental threshold field with decreasing frequency is associated with the growth of the bottom boundary of the $\omega_0' = 1$ resonance zone.

5. Ionization at High Probabilities

So far, we have concentrated our discussion on the threshold fields for ionization, partially for comparison with the available E3D data. Of course, full ionizaton curves exist for both the E1D experiments and the E3D experiments. Relatively little has been said about the E3D data at high ionization probabilities, as these may involve atoms that have substate quantum numbers very different from those of the stretched atoms believed to be most easily ionized. Comparison of the ionization of very non-1D atoms with Q1D calculations might be misleading. On the other hand, our nearly 1D experiments produce ionization curves that are for the same kind of atoms, at all values of the ionization probability. Our ionization curves can be compared with Q1D predictions, with some confidence. They appear to contain more detailed information about the pulsed microwave ionization process. Thus we present our results for the field strengths for 30% and 60% ionization probability in Figure 13, along with our data for 10% probability. The error bars are standard deviations for different runs that often were carried out months or years

apart. Points having no error bars are for single $n_0 = 69$ runs that had remarkably high signal to background ratios and low atom and laser beam intensity drifts.

In all the data in Figure 13, the error bars are small enough to establish the existence of fluctuations in the ionization probability with small variations in frequency. The fluctuations are largest for frequencies between 1.06 and 1.17 in the 30% data, and between 0.8 and 0.9 for the 60% data. These fluctuations are often about 1% wide, or the inverse of the number of field oscillations during the pulse. Thus they may be remanents of sharper, larger fluctuations that have increased widths Fourier-transform limited by the finite interaction time of the atom with the field. Such much sharper fluctuations have been found in recent quantum calculations for frequencies between 0.99 and 1.01 [42].

The overall shapes of the three curves in Figure 13 are remarkably similar. One difference is a discernable shift to lower frequencies of the maximum located near $\omega_0' = 0.69$, as one proceeds from 10% probability to 60% probability. Also, there is an unusual narrow, large maximum close to $\omega_0' = 0.99$ for the 30% data, not seen in the other two data sets. More behavior of these kinds is observed in the frequency dependence of the ionization probability with the scaled field strength held fixed.

Figure 14 shows fixed-F_0 data for $n_0 = 65$, $\omega_0' = 0.57 - 0.73$ and for $n_0 = 69$, $\omega_0' = 0.70 - 1.01$. For $F_0 = 0.02$, there is ionization probability above 10% only for the easy ionization region $\omega_0' = 0.78 - 0.92$ centered near $\omega_0' = 0.85$. At $F_0 = 0.03$ other maxima are detected at $\omega_0' = 0.625$, 0.665 and 0.71. For a further increase in field to $F_0 = 0.04$, these weak maxima have grown and have shifted down discernably in frequency. Local stability (a minimum) centered near 0.695 is evident, as also is the case near 0.57 and 1.00.

The data for $F_0 = 0.05$ are particularly interesting, in that the stability near 0.695 appears to narrow and shift down to 0.685. In addition, a very sharp minimum reduces ionization by 50% extremely close to $\omega_0' = 1.00$. At $F_0 = 0.06$ signs of the stability originally at 0.695 remain, however centered now at 0.675; the sharp minimum has disappeared. Taken together, this evidence again indicates that 1) the region of local stability nominally at 0.68 exhibits an "AC Stark shift" down in frequency produced by the growth with increasing F_0 of the p/q = 1/1 primary resonance zone, and 2) the most central portion of the primary resonance region exhibits ionization particularly sensitive to the parameters.

We have searched for possible effects on the ionization that could arise from resonances in our microwave system, since these could cause structure and "fluctuations" in our data. One search involved measuring the frequencies of these resonances directly, and comparing them with the data. No significant correlation was found with the structure or fluctuations in the data. A second search was to directly compare data for different F_0 and/or n_0 , the data being plotted versus the unscaled and uncorrected raw microwave frequency ω. No significant correlations of the narrow fluctuations were found. Maxima and minima were equally likely to be correlated and anticorrelated with one another.

We also have carried out extensive measurements on the effects of intentionally added microwave noise on the ionization probabilities. These will be reported elsewhere. Our noise study pertinent to the "zero noise" results of the present paper was a classical numerical one. Using the experimental upper bound on the noise field strength, $F_{0N} = 0.0002$ at $n_0 = 69$, we have explored the changes in the C1D ionization probability due to noise for selected frequencies, for the data shown in Figures 6 and 14. The procedure for

introducing the noise is discussed in reference 43. The noise-induced changes were usually less than a few percent in ionization probability, except for a notable exception. Especially at low field strengths, narrow frequency regions at the frequency threshold for "easy ionization", such as $\omega_0' = 0.800$ for $F_0 = 0.015$ in Figure 6, increases in ionization probability by as much as 0.2 were found to occur. This is understandable, as much of the trajectory ensemble is close to the unstable fixed point at the peak of the pulse, and is poised as in Figure 7b to break out along the unstable manifold as shown in Figure 7c. In this situation, a small amount of noise over a relatively long time causes significant ensemble destabilization. No effect was found on the high frequency side of the easy ionization peak, as the dropoff on this side is due to increasing likelihood for separatrix crossing resulting in island trapping. Aside from the ionization enhancement right at frequency thresholds on the low frequency side of the easy ionization regions, the effect of allowable noise was found to be insignificant even for the $F_0 = 0.020$ results shown in Figure 14.

We also have used C1D calculations to explore the potential sensitivity of the experimental ionization probabilities to changes in the experimental parameters. For example, the frequencies for the classical extrema in the frequency range $\omega_0' = 0.55 - 0.74$ were studied for $F_0 = 0.040$ and 0.050. These did not significantly change for static field changes of $\pm$ 1 V/cm, for peak microwave changes of $\pm$ 12 %, for changes in the cutoff n_c of $\pm$ 4, and for changes in the microwave pulse time of $\pm$ 1 ns.

It is interesting to compare the ionization data taken at constant F_0 with the corresponding C1D predictions. These comparisons are shown for four values of F_0 in

Figure 15. The easy ionization region of the data (ω_0' = 0.78 - 0.92) is in reasonable accord with the classical results, as has been found in earlier comparisons of classical and quantum numerical calculations [16]. However, for $F_0 \leq 0.03$ the ionization observed below ω_0' = 0.70 is almost entirely nonclassical. When F_0 = 0.02. this is also true for ω_0' = 0.92 - 1.12. This spans much of the primary resonance island region. We have compared the F_0 = 0.02 data with classical results for the value F_0 = 0.0224 allowed by the experimental uncertainty in F_0. The conclusion then is that ionization outside the easy ionization region usually has probability well above that predicted classically.

When F_0 is increased to 0.04, there is classical ionization over most of the entire frequency range, see Figure 15c. However, there are several notable disagreements with the experimental data. First, an apparent quantum effect suppresses the ionization for ω_0' $\geq$ 1.08. Second, the data exhibit a minimum (of local stability) near ω_0' = 0.68 that is absent classically. We also note in Figure 15d the deviations from the classical model near ω_0' = 1.0. The n_0 = 69 data are higher than classical, while the n_0 = 72 are lower. This is further evidence for large quantum effects very near the center of the primary resonance region. Lastly, the quantum suppression of the classical ionization at ω_0' = 0.57 is in agreement with the discussions above, indicating that quantum local stability is a major feature near this frequency.

To further pursue the question of quantum effects, let us blow up the experimental data of both Figures 13 and 15, and add vertical lines to guide the eye in comparing structure. This is done in Figure 16. If seen, maxima (minima) in Figure 13 should correpond to minima (maxima) in Figure 15, if seen. If appropriate curves in the two figures are locally

chosen so that the microwave fields are similar, many such correspondences can be seen. We have tabulated some of them in Table III, along with corresponding features present in the C1D numerical results shown in Figure 15. Some of the experimental features can be explained classically, with varying degrees of confidence. The experimental minimum at $\omega_0' = 0.68$ is seen to supplant the C1D maximum at 0.65.

The only published Q1D calculations for fixed scaled microwave field strength and varying scaled frequency have recently been reported by Leopold and Richards [16]. Their results involve a physically chosen approximate basis set and the calculations were carried out for $n_0 = 40$. The half sinewave pulse of the present experiments was included, as was a static electric field. We note that they utilized the **A•p** form of the interaction Hamiltonian rather than the **E•r** form used in our C1D calculations. It is unclear to what extent their results should be compared with ours, see Table IV for a comparison of parameters. Nevertheless, for $F_0 = 0.040$ we present in Figure 17 a comparison of their Q1D values of $P_I(\omega_0')$ with our experimental results. The Q1D easy ionization in the frequency range $\omega_0' = 0.72\text{-}0.85$ is in good accord with experiment. However, at higher frequencies experimental ionization probabilities are higher than the Q1D ones. The minimum near $\omega_0' = 1/1$ due to CLS that is observed experimentally is not present in the quantum results. We do note however the nonclassical dip in the Q1D results at $\omega_0' = 0.68$. Although not as pronounced as the experimental one, this dip does support our contention that this minimum is an example of QLS.

6. Further Remarks and Conclusions.

In this paper we have described in some detail how modern nearly one dimensional microwave ionization experiments can be carried out. Significant features are found in the frequency dependence of ionization threshold fields F(10%), with some them being previously detected in 3D experiments. Other features are revealed at high ionization probability, especially when that probability is studied for a number of fixed values of the scaled microwave electric field at the peak of the pulse. Some of these features are correlated with resonance island zones and separatrix zones in phase space. These nearly classical features arise from pulse-induced classical transport processes in phase space, namely 1) electron probability flow into chaotic portions of resonance island zones and 2) separatrix crossing to produce electron probabilty trapping within regular portions of resonance island zones. In the future, preparation of single nondispersive semiclassical Floquet states at the peak of the pulse, of both the separatrix and island center types, may be possible through a careful selection of the parameters n_0, ω_0', F_0, F_{S0} along with the microwave pulse time and envelope.

The authors thank the U. S. National Science Foundation for its support.

REFERENCES

1. J. E. Bayfield and P. M. Koch, Phys. Rev. Lett. 33, 258 (1974); J. E. Bayfield, L. D. Gardner and P. M. Koch, Phys. Rev. Lett. 39, 76 (1977).

2. G. Casati, B. V. Chirikov, I. Guarneri and D. L. Shepelyansky, Phys. Rep. 154, 77 (1987).

3. R. V. Jensen, S. M. Susskind and M. M. Sanders, Phys. Rep. 201, 1 (1991).

4. J. Henkel and M. Holthaus, Phys. Rev. A 45, 1978 (1992).

5. J. Klafter, M. E. Shlesinger and G. Zumofen, Physics Today, February, 1996, see Figure 5 on page 37.

6. G. Radons and R. E. Prange, Phys. Rev. Lett. 61, 1691 (1988),

7. E. J. Heller, Phys. Rev. Lett. 53, 1515 (1984).

8. P. M. Koch and K. A. H. van Leeuwen, Phys. Rep. 255, 289 (1995).

9. J. E. Bayfield and L. A. Pinnaduwage, Phys. Rev. Lett. 54, 313 (1985).

10. J. E. Bayfield and D. W. Sokol, Phys. Rev. Lett. 61, 2007 (1988).

11. J. E. Bayfield, in Quantum Measurement and Chaos, eds. E. R. Pike and S. Sarkar, Plenum Press (1987).

12. J. N. Bardsley, B. Sundaram, L. A. Pinnaduwage and J. E. Bayfield, Phys. Rev. Lett. 56, 1007 (1986).

13. J. E. Bayfield, S. Y. Luie, L. C. Perotti and M. P. Skrzypkowski, Phys. Rev. A 53, R12 (1996).

14. B. E. Sauer, M. R. W. Bellerman and P. M. Koch, Phys. Rev. Lett. 68, 1633 (1992).

15. J. E. Bayfield, S. Y. Luie, L. C. Perotti and M. P. Skrzypkowski, Physica D 83, 46 (1995).

16. J. G. Leopold and D. Richards, J. Phys. B 27, 2169 (1994).

17. K. Dietz, J. Henkel and M. Holthaus, Phys. Rev. A 45, 4960 (1992).

18. D. Delande and A. Buchleitner, Adv. At. Mol. and Opt. Physics 34, 85 (1994).

19. A. Buchleitner and D. Delande, Phys. Rev. Lett. 75, 1487 (1995).

20. J. E. Bayfield, Rev. Sci. Instr. 47, 1450 (1976).

21. P. M. Koch, Phys. Rev. Lett. 41, 99 (1978).

22. P. M. Koch, in Rydberg States of Atoms and Molecules, eds. R. F. Stebbings and F. B. Dunning, Cambridge U. Press (1983).

23. T. S. Green and G. A. Proca, Rev. Sci. Instr. 41, 1409 (1970).

24. G. A. Harrower, Rev. Sci. Instr. 26, 850 (1955).

25. H. D. Zeman, K. Jost and S. Gilad, Rev. Sci. Instr. 42, 485 (1971).

26. S. Y. Luie, Ph.D. Dissertation, University of Pittsburgh (1994).

27. H. A. Bethe and E. E. Salpeter, Quantum Mechanics of One and Two Electron Atoms, Springer-Verlag (1957).

28. R. J. Damburg and V. V. Kolosov, in Rydberg States of Atoms and Molecules, eds. R. F. Stebbings and F. B. Dunning, Cambridge U. Press (1983).

29. D. W. Sokol, Ph.D. Dissertation, University of Pittsburgh (1990).

30. J. R. Hiskes, C. B. Tarter and D. A. Moody, Phys. Rev. 133, A424 (1964).

31. R. Blumel and U. Smilansky, Z. Phys. D 6, 83 (1987).

32. M. Born, The Mechanics of the Atom, Bell, London (1927).

33. R. V. Jensen, Phys. Rev. A 30, 386 (1984).

34. J. G. Leopold and D. Richards, J. Phys. B 24, 1420 (1991).

35. G. Casati, I. Guarneri and D. L. Shepelyansky, IEEE J. Quant. Elect. 24, 1420 (1988).

36. W. H. Press, B. P. Flannery, S. A. Teukolsky and W. T. Vetterling, Numerical Recipes, Cambridge U. Press (1986).

37. K. A. H. van Leeuwen, G. v. Oppen, S. Renwick, J. B. Bowlin, P. M. Koch, R. V. Jensen, O. Rath, D. Richards and J. G. Leopold, Phys. Rev. Lett. 55, 2231 (1985).

38. E. J. Galvez, B. E. Sauer, L. Moorman, P. M. Koch and D. Richards, Phys. Rev. Lett. 61, 2011 (1988).

39. M. R. W. Bellerman, P. M. Koch, D. R. Mariani and D. Richards, Phys. Rev. Lett. 76, 892 (1996).

40. D. Richards, in Classical Dynamics in Atomic and Molecular Physics, T. Grozdanov, P. Grujic and P. Krstic, editors, pages 269-300, World Scientific, Singapore, 1989.

41. R. V. Jensen, M. M. Sanders, M. Saraceno and B. Sundaram, Phys. Rev. Lett. 63, 2771 (1989).

42. J. Zakrzewski, D. Delande and A. Buchleitner, Phys. Rev. Lett. 75, 4015 (1995).

43. J. E. Bayfield, Chaos 1, 110 (1991).

TABLE I

Name	Length (mm)
High field plates "4"	203
Guard plates for the high field	114.3 ± 0.5
Low-field shield plates	203.2 ± 0.5
Preionizer plates	88.9 ± 0.5
Post-ionizer plates	79.4 ± 0.5
State analyzer plates "8"	140.0 ± 0.5

TABLE II

Destabilization features in Figure 6 confirmed due to ionization initiated near p/q unstable fixed points, and stabilization features confirmed due to trapping near p/q stable fixed points.

p/q	Feature	F_0	ω_0'
1/2	Destabilization	0.036	0.4411
1/2	Stabilization	0.050	0.4970
3/5	Destabilization	0.050	0.56672
3/5	Stabilization	0.050	0.5990*
2/3	Destabilization	0.036	0.6143
2/3	Stabilization	0.050	0.6557
3/4	Destabilization	0.036	0.6924
3/4	Stabilization	0.036	0.7176**
1/1	Destabilization	0.015	0.8153
1/1	Stabilization	0.025	0.9940
4/3	Stabilization	0.025	1.3179
3/2	Stabilization	0.025	1.4910

* Ensemble is influenced by p/q=3/5 stable fixed point and by p/q=2/3 unstable fixed point.

** Ensemble is influenced by both p/q=3/4 stable and unstable fixed points.

Table III

Some C1D and E1D Parameters for Stabilization and Destabilization

Process	C1D		E1D		Data Source
	F_0	ω_0'	F_0	ω_0'	
p/q=2/3 destabilization	0.040	0.6239	0.034±0.003	0.630±0.003	F_0(10%)
			0.040	0.622±0.005	F_0=0.040
p/q=2/3 stabilization	0.040	0.6512	Not observed		
Non-C1D stabilization			0.032±0.001	0.667±0.010	F_0(10%)
			0.052±0.002	0.685±0.005	F_0(30%)
			0.040	0.70±0.01	F_0=0.040
			0.050	0.685±0.003	F_0=0.050
p/q=1/1 destabilization	0.020	0.8153	0.011±0.001	0.843±0.020	F_0(10%)
			0.020	0.825±0.020	F_0=0.020
p/q=1/1 stabilization	0.030	0.9995	0.032±0.001	1.000±0.010	F_0(10%)
			0.040	0.992±0.010	F_0=0.040

Table IV.

Parameters for Comparison of the Present Experimental Results with the Available Quantum Numerical Predictions.

Parameter	Q1D Calculations [16]	E1D Experiments
n_0	40	65, 69, 72
ω_0'	0.65 - 1.18	0.56 - 1.16
F_0	0.040	0.040
Pulse Shape	Half Sinewave	Half Sinewave
Pulse Length (Microwave Periods)	100	91 - 146
F_{s0}	0.0193	0.0278 - 0.0418

FIGURE CAPTIONS

Figure 1. Schematic diagram of the laser ODR technique for production of stretched highly excited hydrogen atoms. Atoms initially in the $n,n_1,m = 7,0,0$ state are excited in a strong static electric field F1 up in energy to the 10,0,0 state. The atoms then pass into a low field F2 directed parallel to F1 and are excited to a final state $n_0,0,0$. Here $n_0 = 69$ has been selected.

Figure 2. Schematic diagram of the fast atomic beam apparatus. Apparatus inside the dashed line is viewed from the side, with the rest being a top view. A proton beam produced by a small accelerator (1) is mass-selected by magnet (2). The beam is converted to an atom beam by charge exchange at (3) and then the residual protons and highly excited states are removed by transverse electric fields. The ODR excitation of the stretched atoms is carried out within (4) and (5,6) and their interaction with the microwaves occcurs within the central rectangle inside (7). Static field ionization state-analysis of the atom beam is carried out at (8) and field ionization of those atoms surviving occurs at (10). Protons produced at (10) are charge selected (at 11), energy selected (at 12) and counted by the detector at (13). The magnetic field coils are (14) and item (15) is the CO_2 laser.

Figure 3. The solid line is a state-analyzer field ionization curve for $n_0 = 72$ atoms, while the dots are theoretical expectations.

Figure 4. Schematic of the microwave system for the interaction waveguide. Adjustment of the two variable coaxial attenuators permits independent control of the sinewave and noise levels.

Figure 5. Experimental ionization curves for $n_0 = 60$. At the lower ionization probabilities, the microwave frequencies for the curves from left to right are 16.0 GHz, 16.4 GHz, 16.8 GHz, 17.2 GHz, 17.4 GHz and 18.0 GHz.

Figure 6. Panoramic results of C1D classical numerical calculations for $n_0 = 69$ atoms, at eight different scaled fields F_0 at the peak of the microwave pulse. At each fixed value of scaled frequency, the ionization probability increases with F_0. a) $F_0 = 0.015$, 0.020, 0.025 and 0.030. b) $F_0 = 0.036$, 0.0413, 0.050 and 0.063. Note the logarithmic horizontal scale in b).

Figure 7. Snapshots of the evolution of classical trajectory ensembles in action-angle phase space, overlaid on stroboscopic surfaces of section for the corresponding values of microwave field. Shown is ensemble destabilization near the p/q = 1/2 unstable fixed point, for $\omega_0' = 0.3944$, $T_p = 61.62$ microwave periods, $F_{s0} = 0.0353$ and $F_0 = 0.03600$ at the peak of the microwave pulse. The snapshot time and field values are a) T = 19, F_0 =

0.02967, b) T = 23, F_0 = 0.03318, c) T = 25, F_0 = 0.03443, d) T = 27, F_0 = 0.03532, e) T = 29, F_0 = 0.03584, and f) T = 31, F_0 = 0.035998, near the peak of the pulse. In a) and b), the ensemble is shown to be near the top of the lower region of regular motion. In c), it partially has evolved parallel to an unstable manifold, which influences the further evolution in the chaotic region seen in d)-f).

Figure 8. Ensemble trapping in the region of regular evolution associated with the p/q = 1/2 stable fixed point. The parameters are ω_0' = 0.4444, T_p = 69.42 microwave periods, F_{s0} = 0.0353 and F_0 = 0.05000 at the peak of the microwave pulse. The snapshot time and field values are a) T = 1, F_0 = 0.00226, b) T = 5, F_0 = 0.01122, c) T = 10, F_0 = 0.02186, d) T = 15, F_0 = 0.03139, e) T = 20, F_0 = 0.03932, and f) T = 35, F_0 = 0.049996, near the peak of the pulse. The ensemble is the top curve in a), and cuts through the resonance island in b). In c)-f), much of the ensemble is the "S-shaped" structure within the island.

Figure 9. Ensemble trapping and ensemble destabilization associated with island chains. a) and b): Trapping within the p/q = 4/3 chain occurs for ω_0' = 1.1783, T_p = 108.08 microwave periods, F_{s0} = 0.0353 and F_0 = 0.02500 at the peak of the microwave pulse. a) The ensemble at T = 40 microwave periods, and b) the stroboscopic surface of section at the corresponding field F_0 = 0.01577. c) and d): Ensemble destabilization near the p/q = 2/3 unstable fixed points occurs for the parameters ω_0' = 0.5492, T_p = 85.80 microwave periods, F_{s0} = 0.0353 and F_0 = 0.03600 at the peak of the microwave pulse. c) The ensemble at T = 37, and d) the surface of section at the corresponding field F_0 = 0.03516.

Figure 10. The microwave threshold field for ionization as a function of scaled microwave frequency. Present E1D experimental data are shown with their standard deviations from averaging over runs. Previously reported E3D experimental data are included for 9.904 GHz (dots), 9.923 GHz (inverted triangles) and 36.02 GHz (triangles). For comparison of structure (only) with the present data taken with a static electric field present, the E3D data are presented in a mixed-plot mode, see text.

Figure 11. The experimental ionization threshold field for n_0 = 80 atoms at scaled frequencies near 4/3. Open and closed circles are data taken on different days.

Figure 12. A comparison of observed values of the ionization threshold field with the calculated separatrix location functions (triangles). Circular dots are n_0 = 65 data while the squares are n_0 = 69 data.

Figure 13. The experimental scaled microwave field strengths for X% ionization probability. From bottom to top, X = 10, 30, and 60. Available points for n_0 = 65, 69 and 72 are included. The error bars are standard deviations of averages over multiple runs.

Figure 14. Frequency dependence of the experimental ionization probability at fixed scaled microwave field F_0 , for n_0 = (a) 65 and (b) 69. For each figure, F_0 = 0.020, 0.030, 0.040 0.050 and 0.060 from bottom to top,.

Figure 15. Conparisons of experimental and classical numerical results for the ionization probability at fixed scaled field. Data for n_0 = 65, 69 and 72 are included. The curve(s) through points containing error bars are experimental. The values of F_0 are (a) 0.020, (b) 0.030, (c) 0.040 and (d) 0.050. Numerical results for different n_0 sometimes do not agree well. This arises from experimentally-imposed differences in scaled static field and scaled microwave pulse time, see text.

Figure 16. Comparisons of scaled fields for fixed ionization probability (top) with ionization probabilities at fixed scaled fields (bottom). In the former, the curves are for 10%, 30% and 60% probability from bottom to top. (a) n_0 = 65 data, including fixed field results for F_0 = 0.04 and 0.05; (b) n_0 = 65 and 69 data, including fixed field results for F_0 = 0.02 and 0.03; (c) n_0 = 69 and 72 data, including fixed field results for F_0 = 0.02 and 0.03.

Figure 17. Comparison of the present experimental data (points and error bars) with the quantum numerical results of Leopold and Richards [16]. The latter were computed for n_0 = 40, see text. Both results are for F_0 = 0.04.

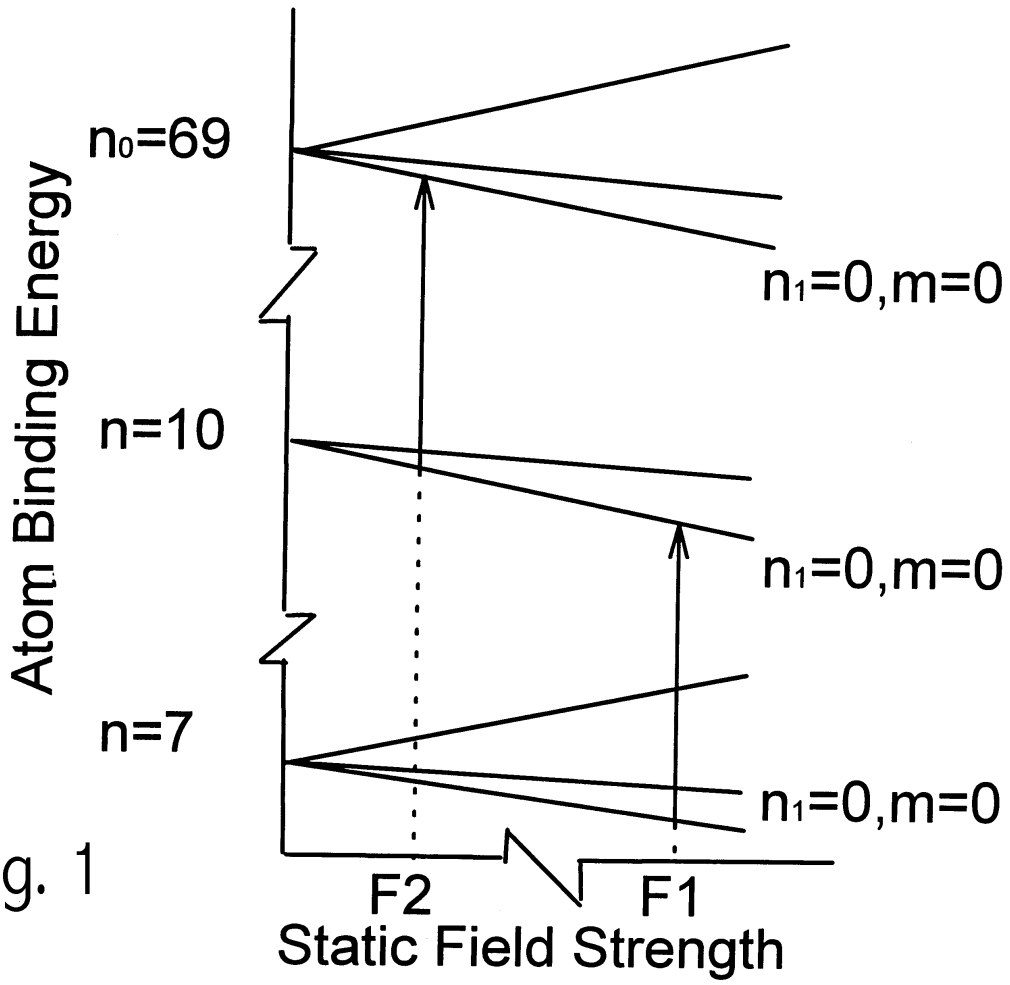
Atom Binding Energy
n0=69
n=10
n=7
n1=0,m=0
n1=0,m=0
n1=0,m=0
F2
F1
Static Field Strength

Fig. 1

Fig. 2

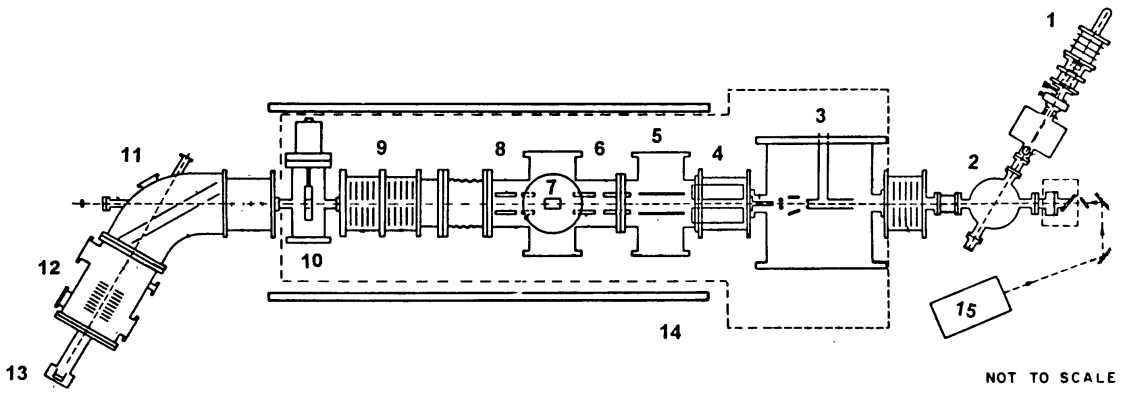

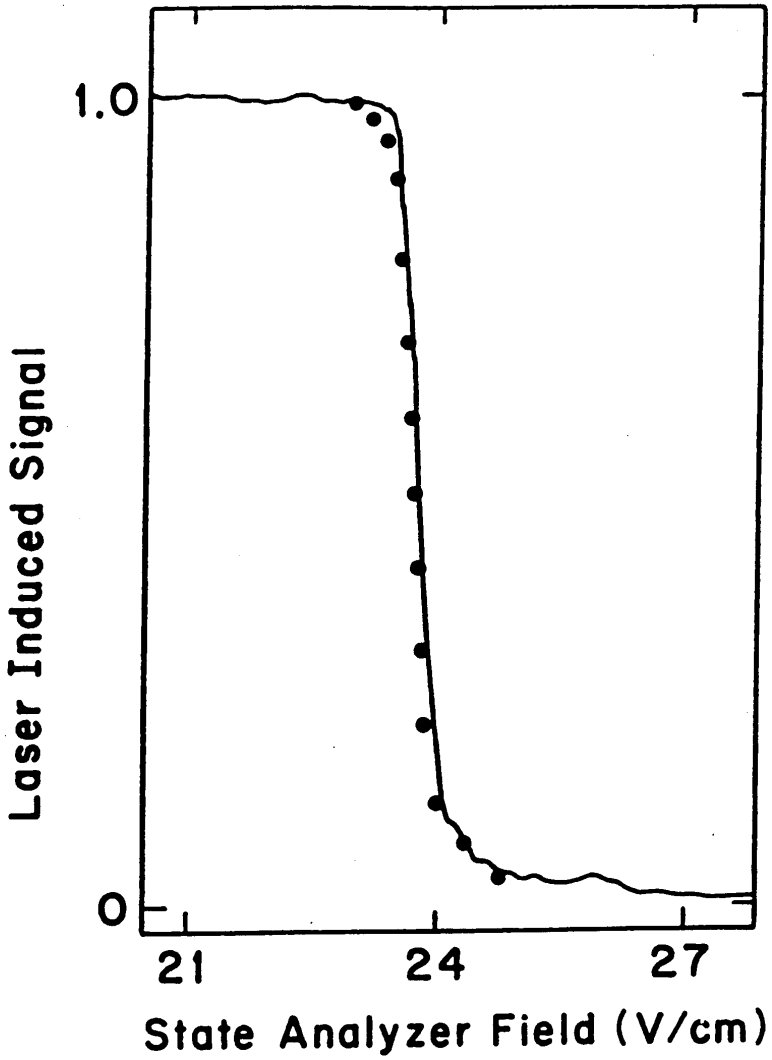

Fig. 3

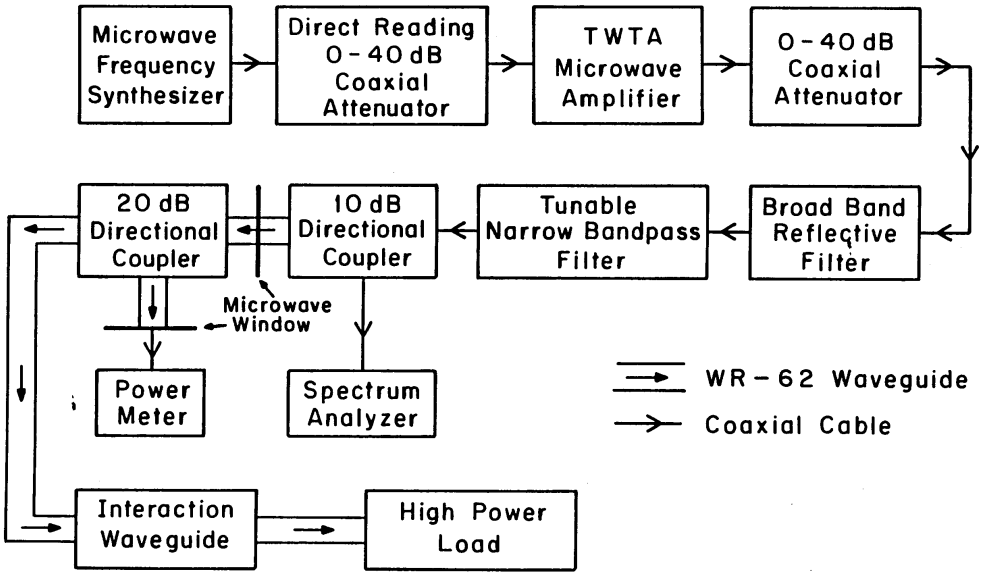
Microwave Frequency Synthesizer
Direct Reading 0-40 dB Coaxial Attenuator
TWTA Microwave Amplifier
0-40 dB Coaxial Attenuator
20 dB Directional Coupler
10 dB Directional Coupler
Tunable Narrow Bandpass Filter
Broad Band Reflective Filter
Microwave Window
Power Meter
Spectrum Analyzer
WR-62 Waveguide
Coaxial Cable
Interaction Waveguide
High Power Load

Fig. 4

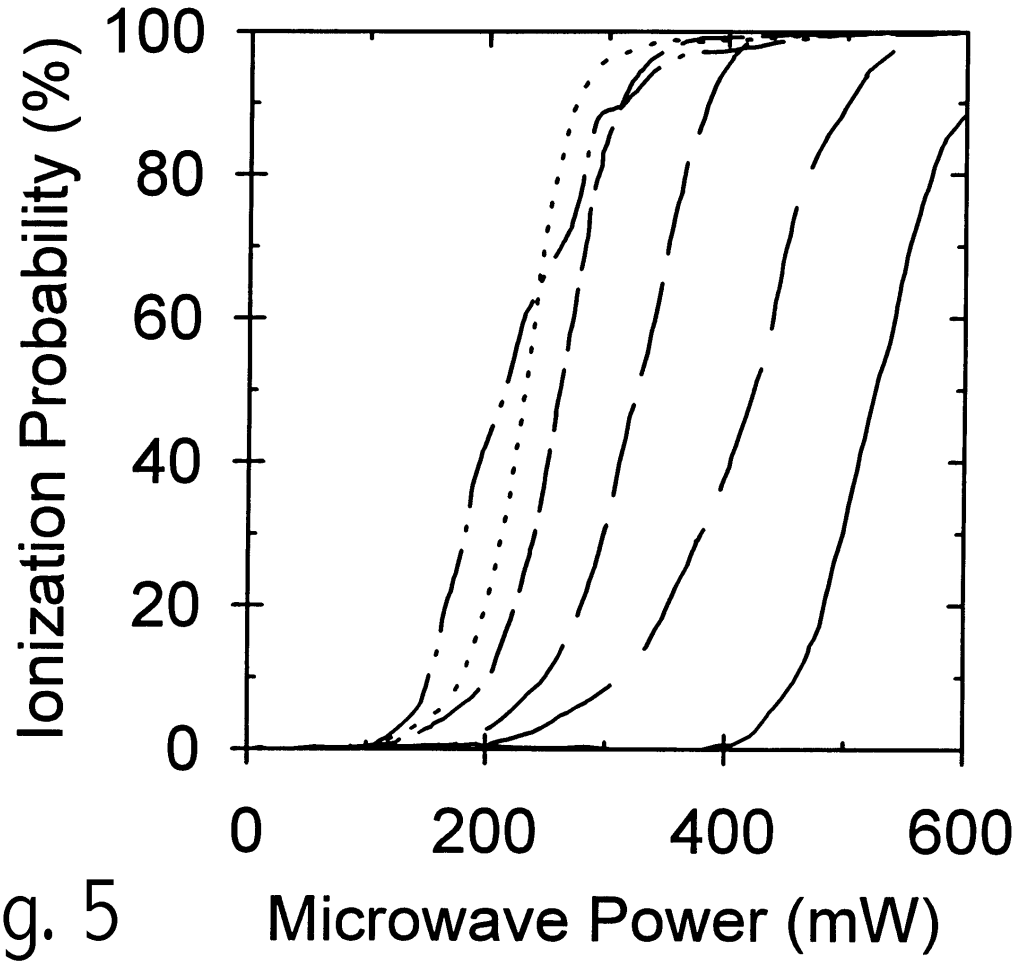
Ionization Probability (%)
100
80
60
40
20
0
0
200
400
600
Microwave Power (mW)

Fig. 5

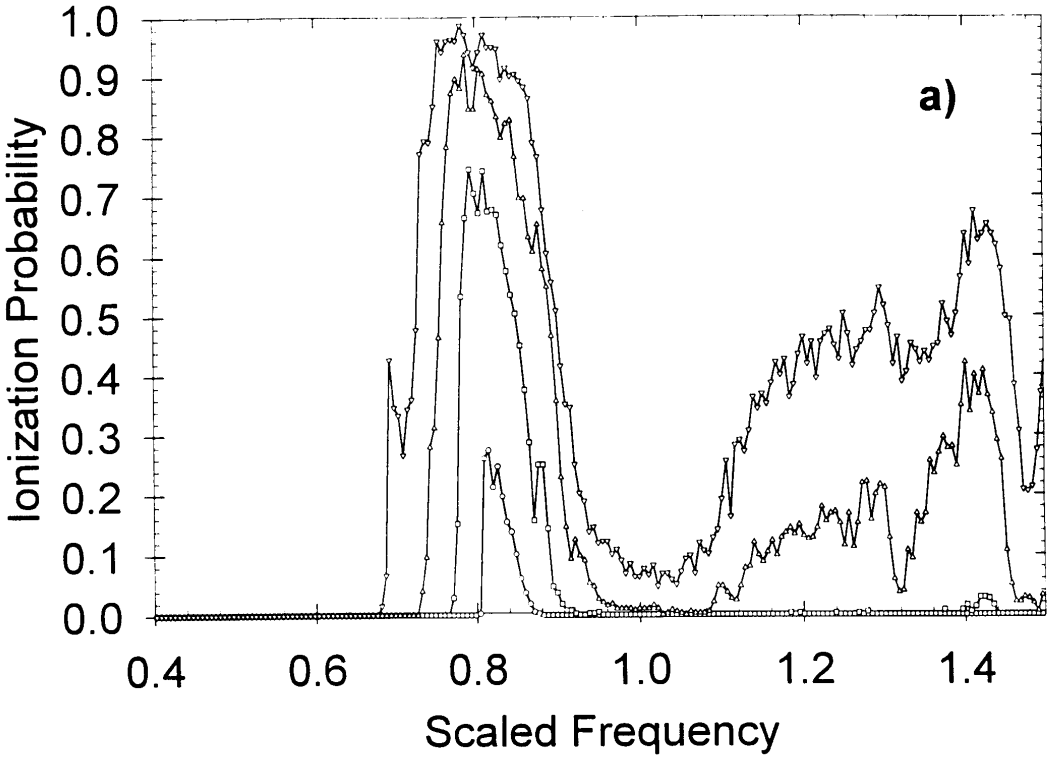
Ionization Probability
1.0
0.9
0.8
0.7
0.6
0.5
0.4
0.3
0.2
0.1
0.0
a)
0.4
0.6
0.8
1.0
1.2
1.4
Scaled Frequency

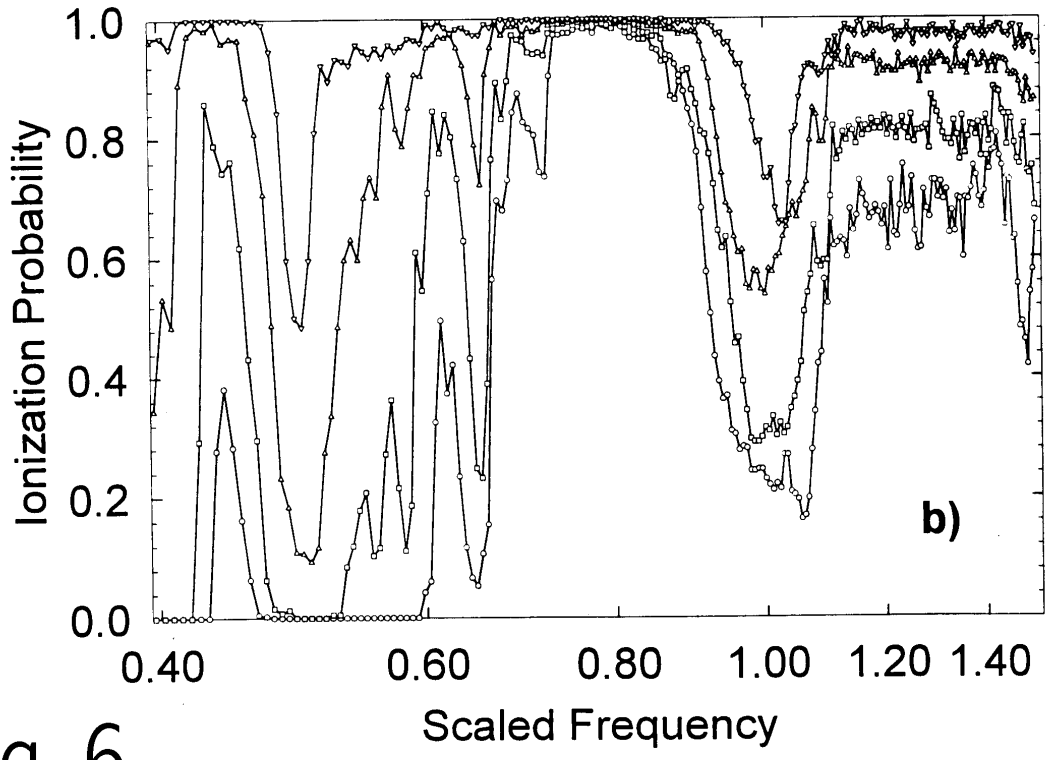
Ionization Probability
1.0
0.8
0.6
0.4
0.2
0.0
b)
0.40
0.60
0.80
1.00
1.20
1.40
Scaled Frequency

Fig. 6

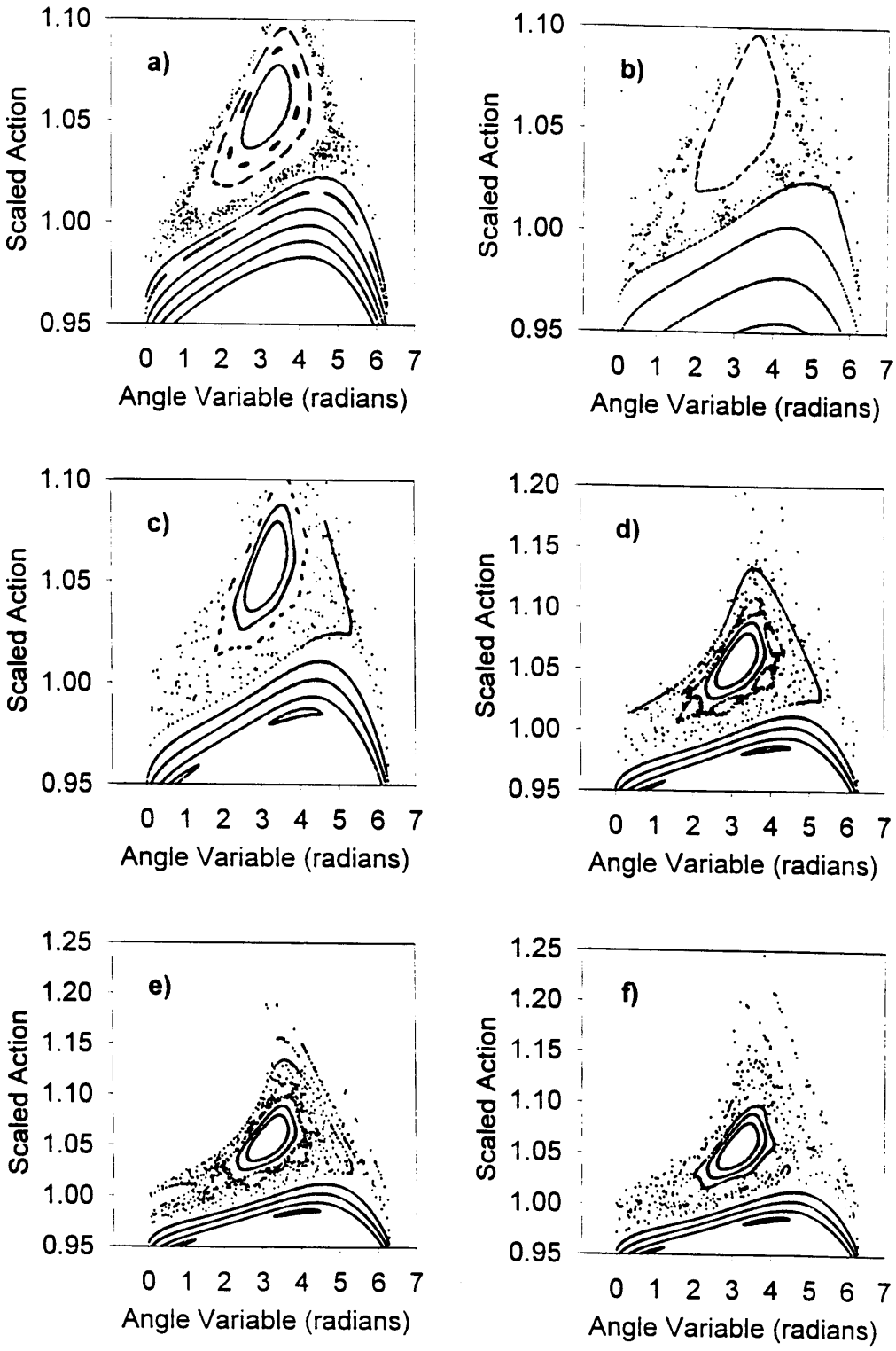
a)
b)
c)
d)
e)
f)
Scaled Action
Angle Variable (radians)
1.10
1.05
1.00
0.95
1.20
1.15
1.25
0 1 2 3 4 5 6 7

Fig. 7

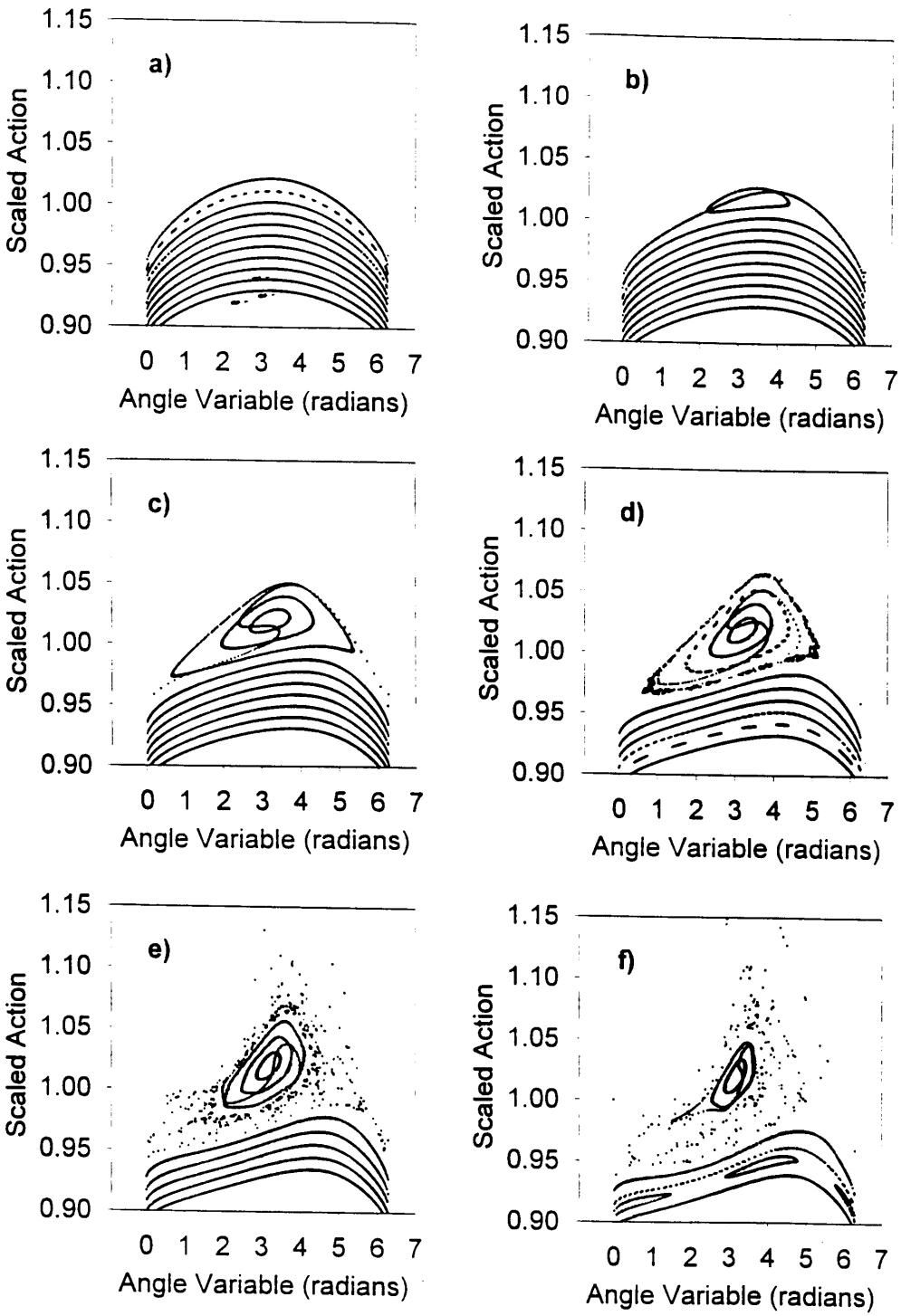
a)
b)
c)
d)
e)
f)
Scaled Action
Angle Variable (radians)
1.15
1.10
1.05
1.00
0.95
0.90
0 1 2 3 4 5 6 7

Fig. 8

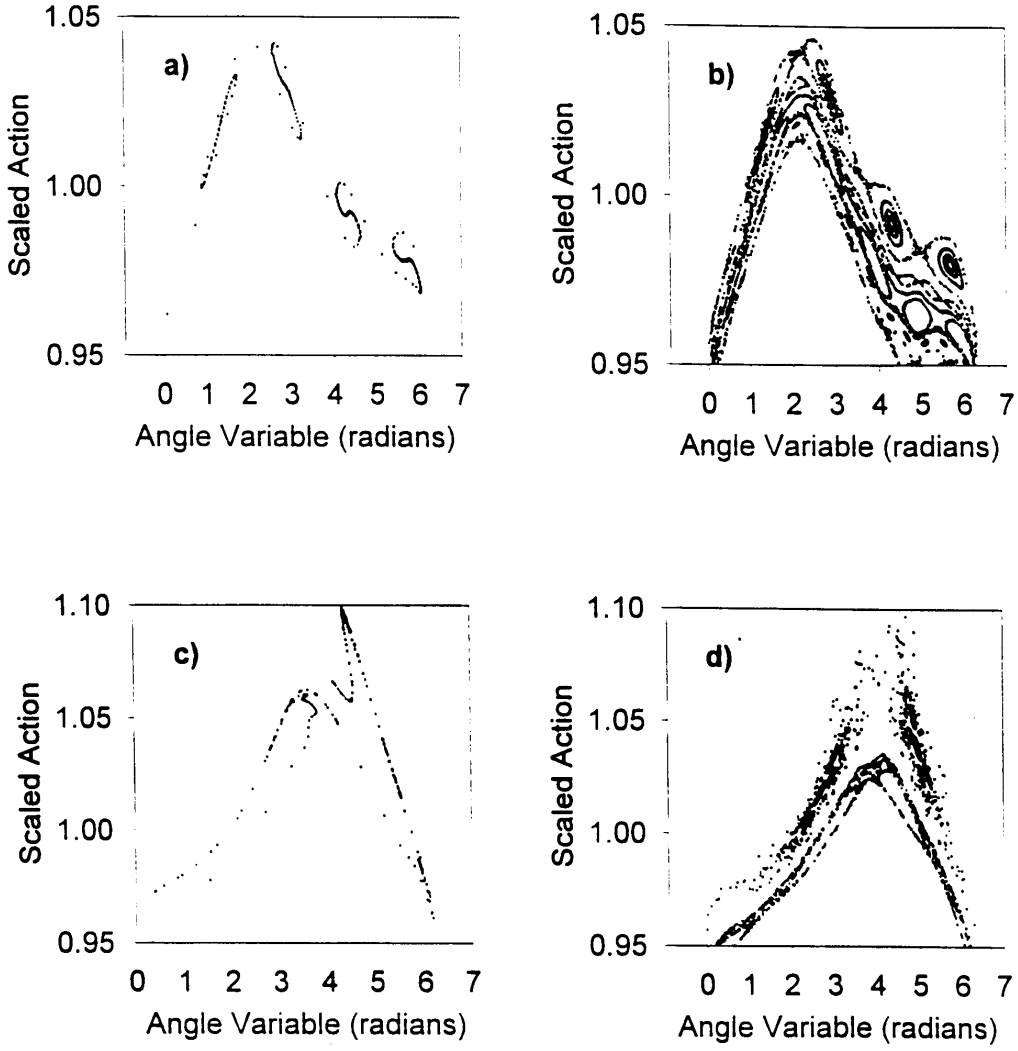
a)
b)
c)
d)
Scaled Action
Angle Variable (radians)
1.05
1.00
0.95
1.10
0 1 2 3 4 5 6 7

Fig. 9

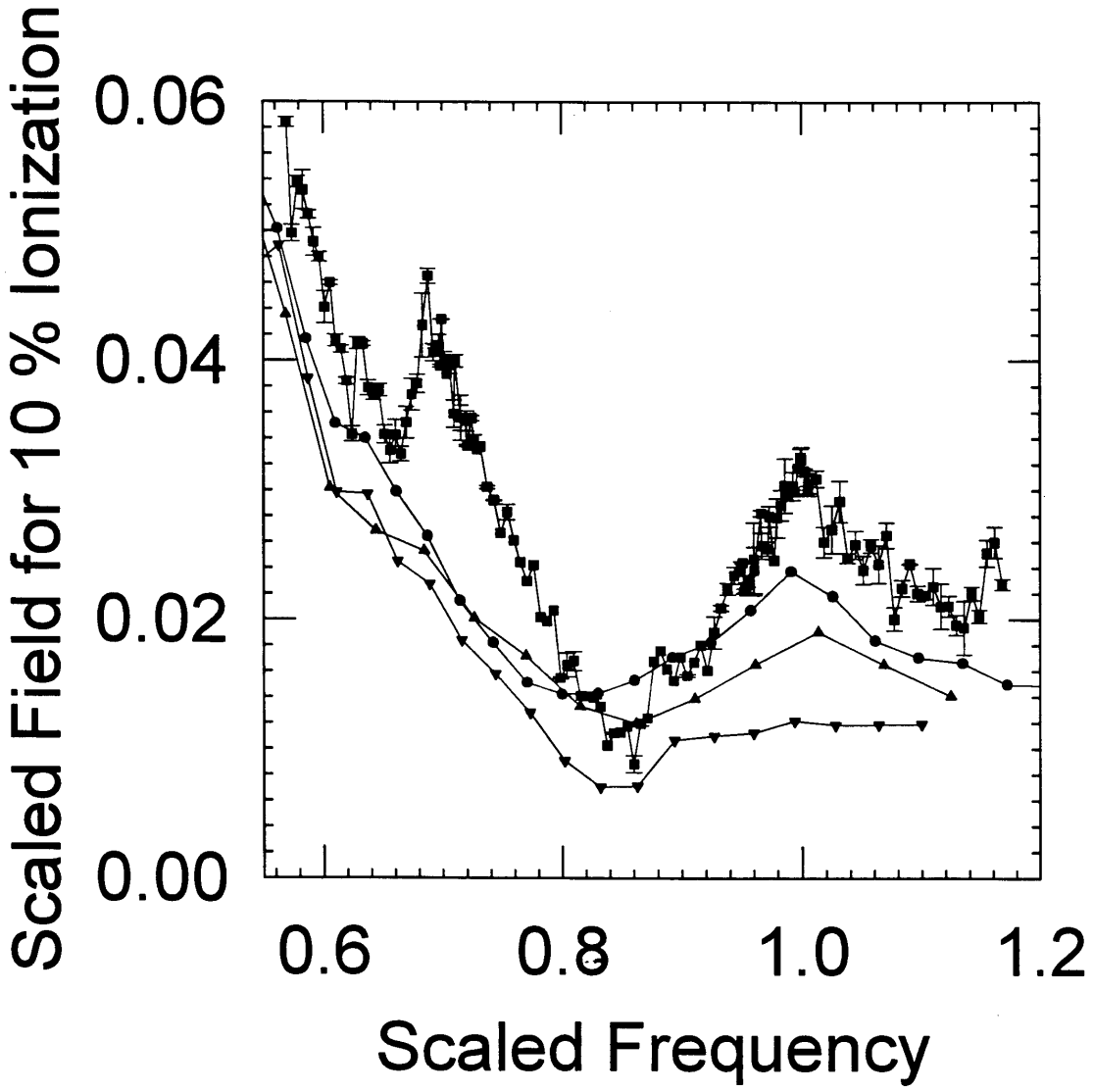
Scaled Field for 10 % Ionization
0.06
0.04
0.02
0.00
0.6
0.8
1.0
1.2
Scaled Frequency

Fig. 10

Fig. 11

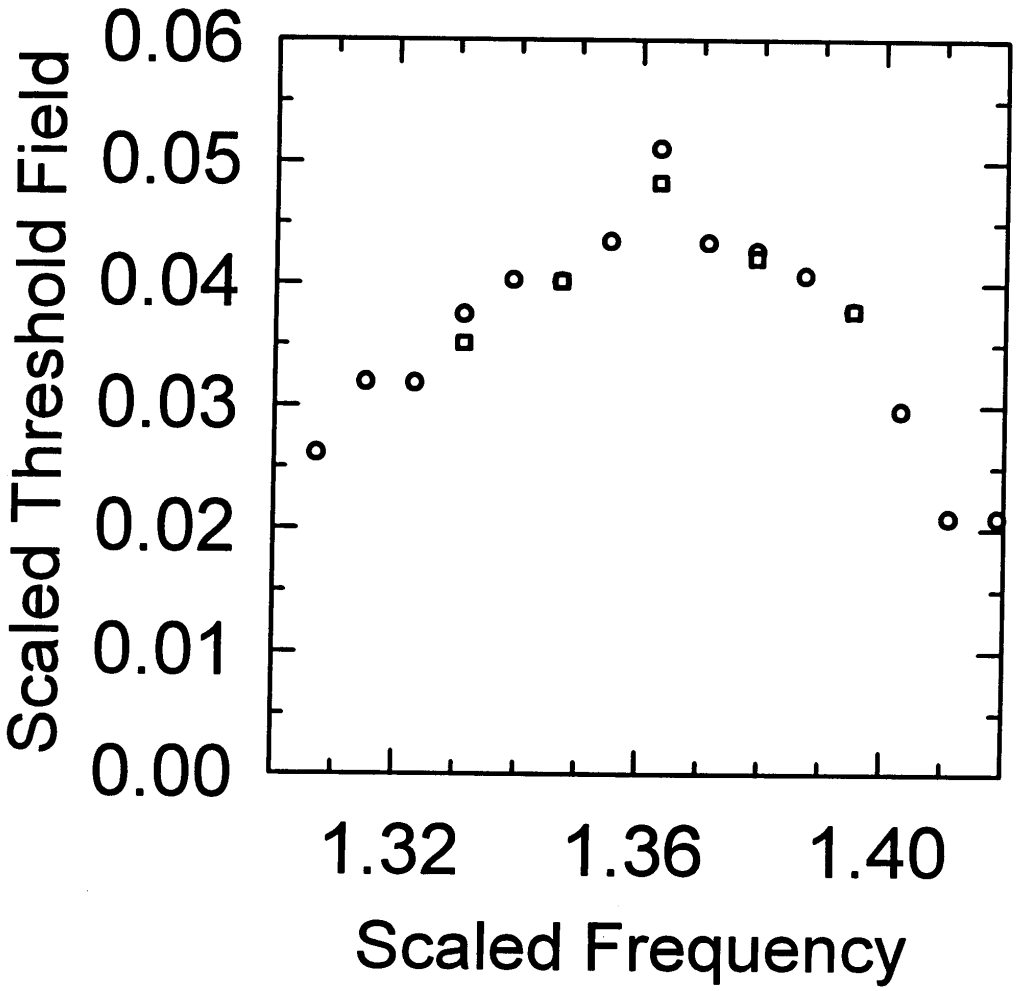
Scaled Threshold Field
0.06
0.05
0.04
0.03
0.02
0.01
0.00
1.32
1.36
1.40
Scaled Frequency

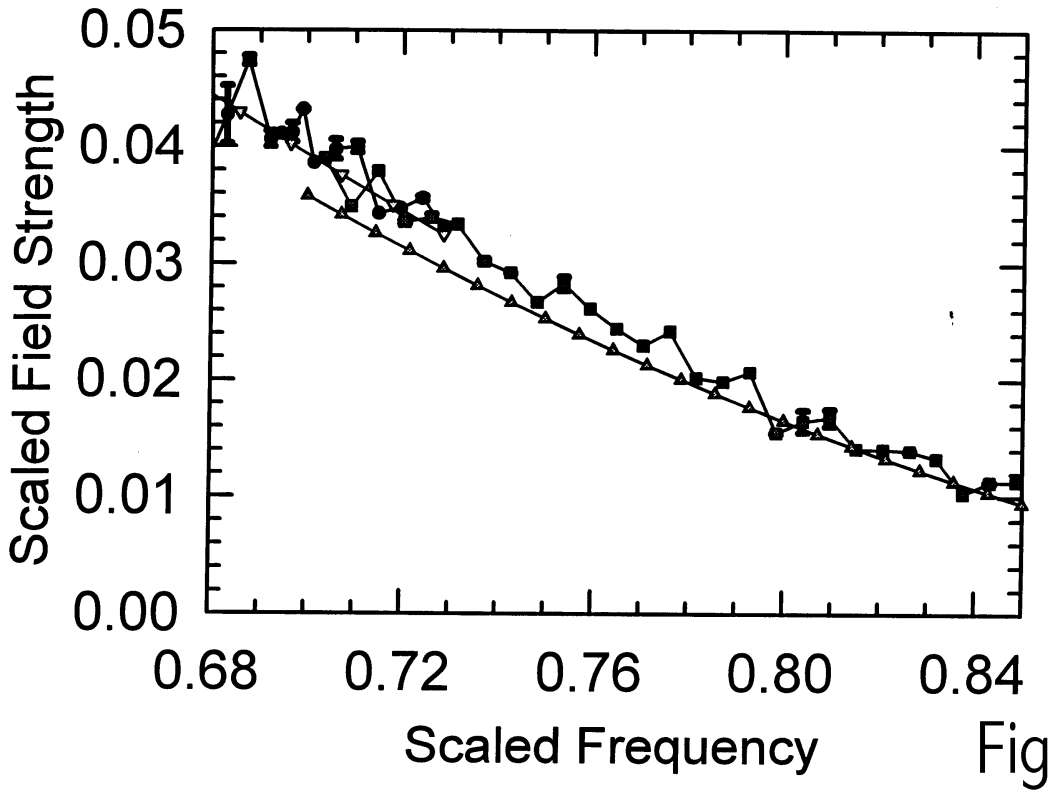
0.05
0.04
0.03
0.02
0.01
0.00
Scaled Field Strength
0.68
0.72
0.76
0.80
0.84
Scaled Frequency

Fig. 12

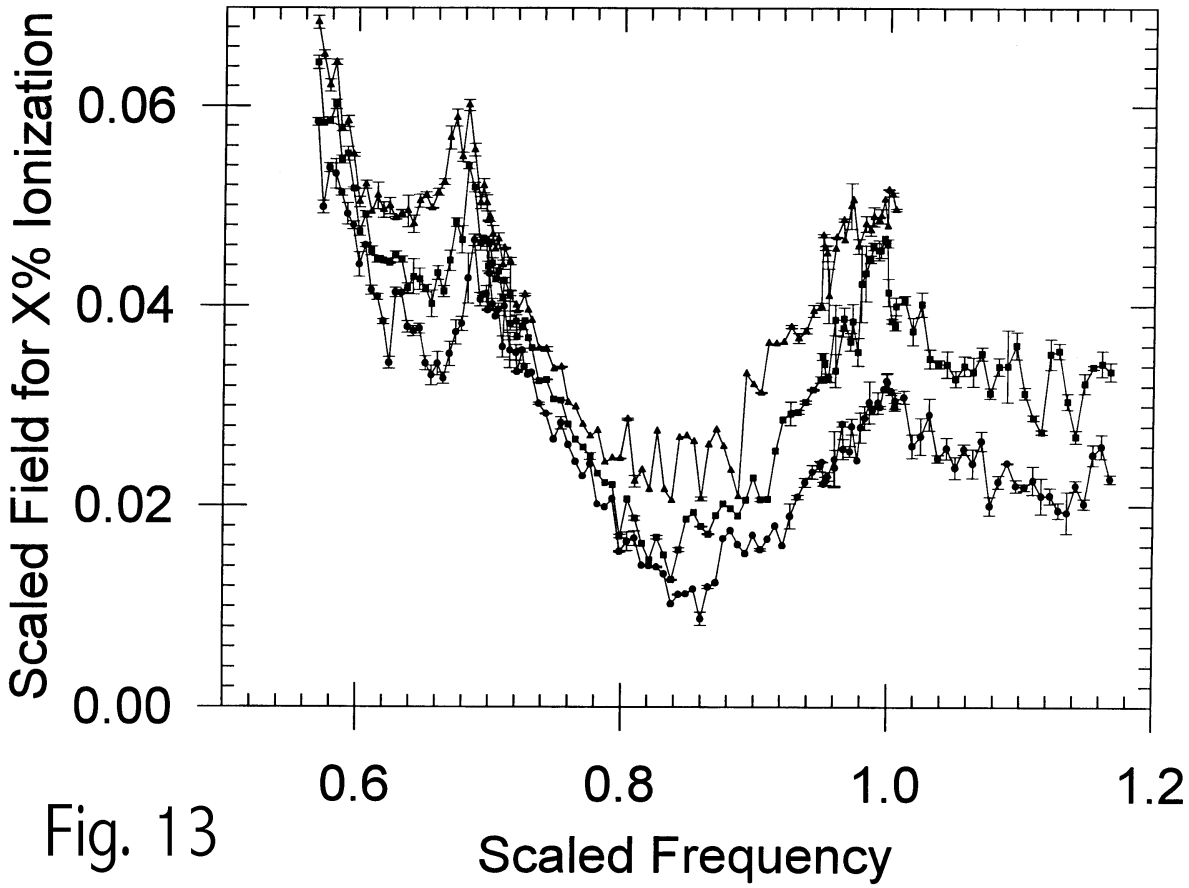
Scaled Field for X% Ionization
0.06
0.04
0.02
0.00
0.6
0.8
1.0
1.2
Scaled Frequency

Fig. 13

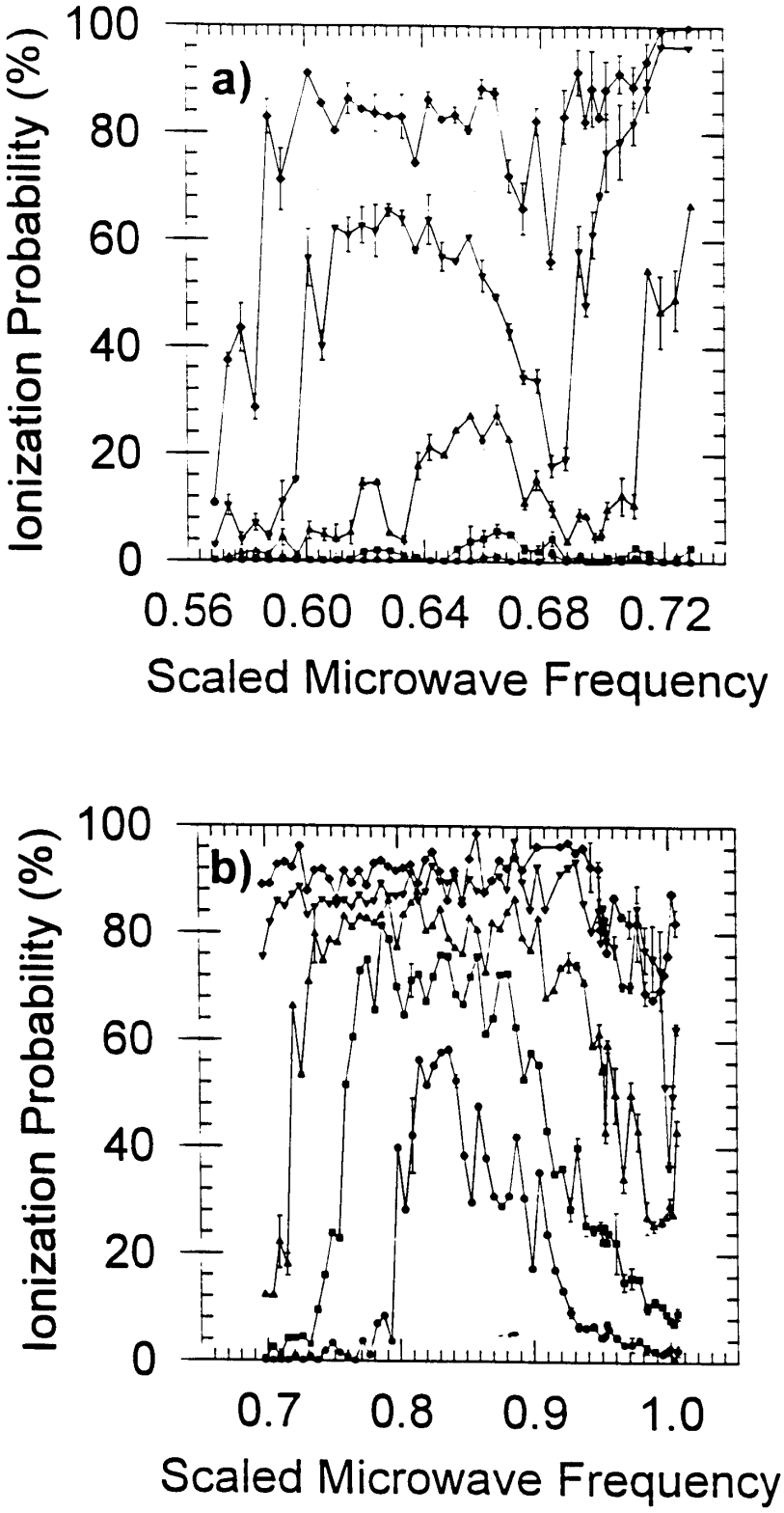
a)
Ionization Probability (%)
100
80
60
40
20
0
0.56 0.60 0.64 0.68 0.72
Scaled Microwave Frequency
b)
Ionization Probability (%)
100
80
60
40
20
0
0.7 0.8 0.9 1.0
Scaled Microwave Frequency

Fig. 14

Fig. 15

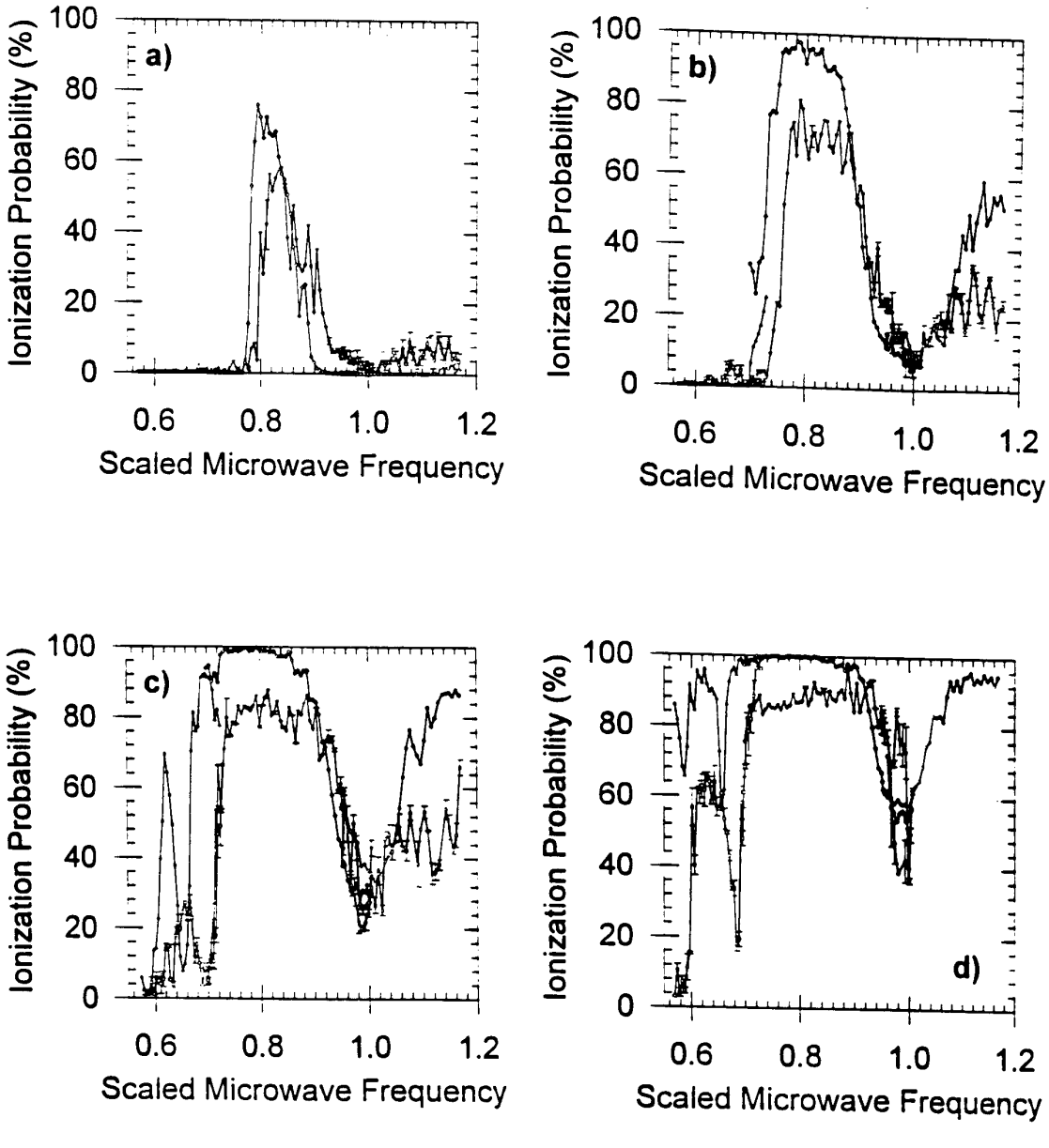
a)
b)
c)
d)
Ionization Probability (%)
Scaled Microwave Frequency
0
20
40
60
80
100
0.6
0.8
1.0
1.2

Fig. 16

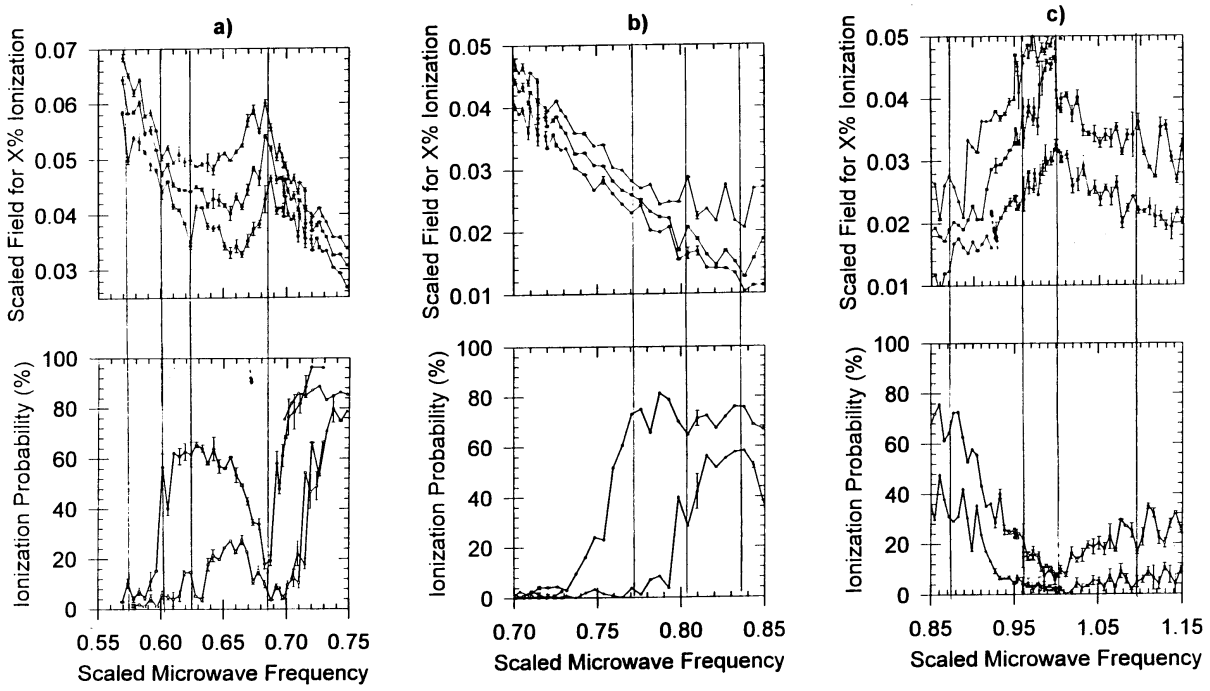
a)
b)
c)
Scaled Field for X% Ionization
Ionization Probability (%)
Scaled Microwave Frequency
0.07
0.06
0.05
0.04
0.03
0.02
0.01
100
80
60
40
20
0
0.55 0.60 0.65 0.70 0.75
0.70 0.75 0.80 0.85
0.85 0.95 1.05 1.15

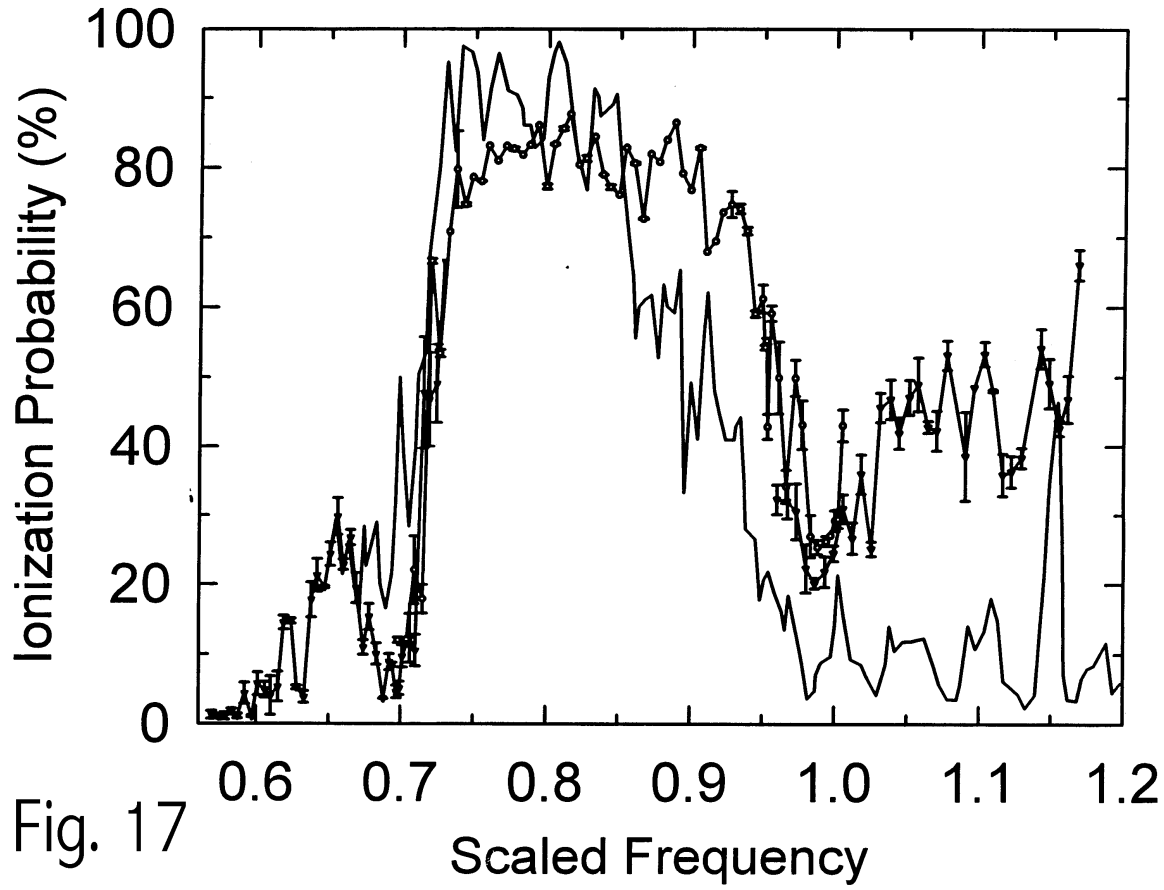
Ionization Probability (%)
Scaled Frequency
100
80
60
40
20
0
0.6 0.7 0.8 0.9 1.0 1.1 1.2

Fig. 17